

# Chemo-Archaeological Downsizing in a Hierarchical Universe: Impact of a Top Heavy IGIMF

I. D. Gargiulo<sup>1\*</sup>, S. A. Cora<sup>1,2,3</sup>, N. D. Padilla<sup>4,5</sup>, A. M. Muñoz Arancibia<sup>4</sup>, A. N. Ruiz<sup>3,6,7</sup>, A. A. Orsi<sup>4,5</sup>, T. E. Tecce<sup>4,5</sup>, C. Weidner<sup>8,9</sup> and G. Bruzual<sup>10</sup>

<sup>1</sup>*Instituto de Astrofísica de La Plata (CCT La Plata, CONICET, UNLP), Paseo del Bosque s/n, B1900FWA, La Plata, Argentina.*

<sup>2</sup>*Facultad de Ciencias Astronómicas y Geofísicas, Universidad Nacional de La Plata, Paseo del Bosque s/n, B1900FWA, La Plata, Argentina.*

<sup>3</sup>*Consejo Nacional de Investigaciones Científicas y Técnicas, Rivadavia 1917, C1033AAJ Buenos Aires, Argentina.*

<sup>4</sup>*Instituto de Astrofísica, Pontificia Universidad Católica de Chile, Av. Vicuña Mackenna 4860, Santiago, Chile.*

<sup>5</sup>*Centro de Astro-Ingeniería, Pontificia Universidad Católica de Chile, Av. Vicuña Mackenna 4860, Santiago, Chile.*

<sup>6</sup>*Instituto de Astronomía Teórica y Experimental (CCT Córdoba, CONICET, UNC), Laprida 854, X5000BGR, Córdoba, Argentina.*

<sup>7</sup>*Observatorio Astronómico de Córdoba, Universidad Nacional de Córdoba, Laprida 854, X5000BGR, Córdoba, Argentina.*

<sup>8</sup>*Instituto de Astrofísica de Canarias, Calle Vía Láctea, E38205 - La Laguna (Tenerife), España.*

<sup>9</sup>*Departamento de Astrofísica, Universidad de La Laguna (ULL), E-38206 La Laguna, Tenerife, España.*

<sup>10</sup>*Centro de Radioastronomía y Astrofísica, UNAM, Campus Morelia, México.*

Accepted ... . Received ... ; in original form ...

## ABSTRACT

We make use of a semi-analytical model of galaxy formation to investigate the origin of the observed correlation between  $[\alpha/\text{Fe}]$  abundance ratios and stellar mass in elliptical galaxies. We implement a new galaxy-wide stellar initial mass function (Top Heavy Integrated Galaxy Initial Mass Function, TH-IGIMF) in the semi-analytic model SAG and evaluate its impact on the chemical evolution of galaxies. The SFR-dependence of the slope of the TH-IGIMF is found to be key to reproducing the correct  $[\alpha/\text{Fe}]$ -stellar mass relation. Massive galaxies reach higher  $[\alpha/\text{Fe}]$  abundance ratios because they are characterized by more top-heavy IMFs as a result of their higher SFR. As a consequence of our analysis, the value of the minimum embedded star cluster mass and of the slope of the embedded cluster mass function, which are free parameters involved in the TH-IGIMF theory, are found to be as low as  $5 M_{\odot}$  and 2, respectively. A mild downsizing trend is present for galaxies generated assuming either a universal IMF or a variable TH-IGIMF. We find that, regardless of galaxy mass, older galaxies (with formation redshifts  $\gtrsim 2$ ) are formed in shorter time-scales ( $\lesssim 2$  Gyr), thus achieving larger  $[\alpha/\text{Fe}]$  values. Hence, the time-scale of galaxy formation alone cannot explain the slope of the  $[\alpha/\text{Fe}]$ -galaxy mass relation, but is responsible for the big dispersion of  $[\alpha/\text{Fe}]$  abundance ratios at fixed stellar mass. We further test the hypothesis of a TH-IGIMF in elliptical galaxies by looking into mass-to-light ratios, and luminosity functions. Models with a TH-IGIMF are also favoured by these constraints. In particular, mass-to-light ratios agree with observed values for massive galaxies while being overpredicted for less massive ones; this overprediction is present regardless of the IMF considered.

**Key words:** Galaxies: abundances - Galaxies: formation - Methods: numerical

## 1 INTRODUCTION

The chemical signatures imprinted in stellar populations are key features in the understanding of the formation and evolution of galaxies. The alpha-element abundance relative to iron has been

recognized for a long time as an indicator of the formation time-scale of stellar populations. It is well known that the alpha-elements are produced by alpha capture exclusively in core-collapse supernovae (SNe CC), whose progenitors have lifetimes of tens of Megayears, while Fe and Fe-peak elements are mainly the yields of type Ia supernovae (SNe Ia), whose progenitors are long lived ( $0.5 - 3$  Gyr, Greggio 2005). A composite stellar population with

\* E-mail: gargiulo@fcaglp.unlp.edu.ar

an excess of alpha-elements relative to iron is therefore assumed to form in a short period of time ( $\lesssim 1$  Gyr) (Matteucci 1994), given that the bulk of stars in the system form before the interstellar medium (ISM) is contaminated with the SNe Ia yields. The early works of Tinsley (1976, 1979) already considered this abundance ratio in order to explain the formation time-scales of the solar neighbourhood and the Milky Way stellar halo. This argument has been also considered to explain the trend observed among elliptical galaxies in which more massive ellipticals (with higher velocity dispersions) have systematically higher alpha-elements to iron ratios (e.g. Worthey et al. 1992). Faber (1973) first observed that some absorption features related to the abundance of Mg increase monotonically with increasing luminosity. Since then, a large amount of work has been done measuring alpha-element abundances to study this trend in all sort of environments (e.g. Worthey et al. 1992; Trager et al. 2000; Kuntschner 2000; Bernardi et al. 2006; Sánchez-Blázquez et al. 2006; Spolaor et al. 2010; Thomas et al. 2010).

In the context of the  $\Lambda$ -CDM paradigm, the observed trend of  $[\alpha/\text{Fe}]$  as a function of mass could be considered troublesome. In this framework, the growth of structure is hierarchical. Dark matter (DM) haloes form via dissipationless gravitational collapse (White & Rees 1978) and grow in a bottom-up fashion, with more massive haloes taking longer periods of time to build-up their masses. Considering that galaxies form in the centre of DM haloes, a priori it is not expected that more massive galaxies have higher abundances of  $\alpha$ -elements relative to iron. Nevertheless, the existence of baryonic processes like gas cooling, star formation (SF) and feedback from SNe and active galactic nuclei (AGN) can detach the actual formation of the galaxy from the assembly of its parent DM halo. This “anti-hierarchical” behavior, usually called *downsizing*, manifests in different ways in galaxies: the characteristic mass of star forming galaxies increases with redshift (e.g. Cowie & Barger 2008), the evolution of the stellar mass functions seems to indicate that less massive galaxies assembly their mass at later times (e.g. Pérez-González et al. 2008), more massive galaxies have older stellar populations than less massive ones (e.g. Gallazzi et al. 2005). Fontanot et al. (2009) classify the different observational manifestations of downsizing, suggesting the possibility that not all these phenomena are related to the same underlying physical process. In particular, they coined the term *chemoarchaeological downsizing* to refer to the trend of abundance ratios with stellar mass shown by elliptical galaxies.

The pointed tension between observations and the hierarchical paradigm has been addressed by different groups using analytic and semi-analytic models of galaxy formation (SAMs). Thomas (1999) was the first in modelling the chemical enrichment of elliptical galaxies within the framework of hierarchical galaxy formation, but considering a closed box model for each galaxy and ignoring the merger history of galaxies by using pre-calculated star formation histories. He fails to reproduce the observed trend of  $[\alpha/\text{Fe}]$  versus velocity dispersion. Nagashima et al. (2005) study the metal enrichment of elliptical galaxies using a semi-analytic model with merger trees. They find that a top heavy initial mass function (IMF) in starbursts is needed in order to reproduce the observed  $[\alpha/\text{Fe}]$  abundance ratio in  $L_*$  ellipticals, but none of their models reproduce the observed trend of this ratio with velocity dispersion,  $\sigma$ .

Pipino et al. (2009) focussed on the  $[\alpha/\text{Fe}]$ -stellar mass relation in elliptical galaxies by including the enrichment of supernovae type Ia and II, and of low- and intermediate- mass stars, as well as the corresponding delay times for SNe Ia in the semi-analytic model of galaxy formation GalICS. They find a better agreement

with the observed  $[\alpha/\text{Fe}]$ - $\sigma$  relation when taking into account AGN feedback in their models, although still marginal. Calura & Menci (2009) implement a chemical model on top of the star formation histories extracted from a semi-analytic model, and evaluate the impact on the  $[\alpha/\text{Fe}]$ - $\sigma$  relation of the AGN feedback and an ad-hoc variable IMF that becomes top heavy in starbursts, finding that they are both needed to obtain a slope in the relation similar to the observed one. This was the first attempt to include a variable IMF in a semi-analytic model to study the  $[\alpha/\text{Fe}]$  ratios in ellipticals. A similar assumption about the IMF has been considered by Baugh et al. (2005) to explain the number counts of submillimeter galaxies at high redshift. Later on, Calura & Menci (2011) mention the importance of the harassment of satellite galaxies at high redshift as a trigger of SF in the progenitors of massive galaxies that form stars enhanced in  $\alpha$ -elements, contributing to build up the relation. Arrighi et al. (2010) also analyse the  $[\alpha/\text{Fe}]$ -mass relation by using the semi-analytic model of Somerville et al. (2008) that includes AGN feedback, in which they implement a chemical enrichment model that involves SNe Ia and SNe II yields and the corresponding delay times for the SNe Ia explosions. They find a good agreement with observations by combining a shallower slope for the IMF and a lower SNe Ia fraction. All the results obtained from semi-analytic models of galaxy formation and evolution suggest that the time-scale argument, which compares the time-scales of SF and metal ejection from SNe, might be insufficient to explain the build-up of the  $[\alpha/\text{Fe}]$ -mass relation of early type galaxies, supporting the importance of the role of the IMF.

Numerous works are being published that show the need to explore alternative and variable stellar initial mass functions. The stellar IMF has direct consequences on the evolution of galaxies. It determines the ratio of massive stars to low and intermediate-mass stars, imprinting the chemical abundance ratios of stellar populations in galaxies (Lucatello et al. 2005; Köppen et al. 2007), and establishing the amount of reheated mass deposited in the ISM by SNe explosions. It also determines the mass-to-light ratio (M/L) of galaxies, given that stars with different initial stellar masses contribute with very different amounts of light along their lives. In the last decade, a formalism for a galaxy-wide stellar IMF has been developed (see Kroupa et al. 2013, or Subsection 2.3 of this paper), where the instantaneous star formation rate (SFR) of galaxies determines the final shape of the integrated IMF. Recchi et al. (2009) evaluate the influence on the  $[\alpha/\text{Fe}]$ - $\sigma$  relation of the galaxy-wide integrated galactic initial mass function (IGIMF, Kroupa & Weidner 2003) implemented in an analytical model of chemical enrichment of galaxies. They find that the downsizing effect (shorter duration of the SF in larger galaxies) must be present to reproduce the observed trend, although it must be milder than the one inferred by Thomas et al. (2005) on the basis of the observational  $[\alpha/\text{Fe}]$ - $\sigma$  relation. Several simplifying assumptions have been adopted in their work. Moreover, they do not include the effect of a top heavy version of the IGIMF (TH-IGIMF) (Weidner et al. 2011, 2013). This particular IMF has been tested by Fontanot (2014) in the semi-analytic model MORGANA evaluating its impact on the stellar mass functions and star formation rates. These results are compared with those obtained from other IMF with different dependencies on galaxy properties and environment, finding that the predicted galaxy properties are mainly affected by an increasing Top-Heavy IMF at increasing star formation rates.

The aim of this work is to address the chemical evolution of galaxies in the framework of the  $\Lambda$ -CDM paradigm, tackling the problem of  $\alpha$ -element enrichment in elliptical galaxies. We evaluate the impact of the new theory of TH-IGIMF, never considered so

far for this particular issue. We also analyse the influence of the TH-IGIMF in the luminosity function and the mass-to-light ratios of elliptical galaxies analyzing the tilt of the fundamental plane (M/L vs M). For this purpose, we use the state of the art semi-analytic model SAG (acronym for Semi-Analytic Galaxies) that couples the most relevant ingredients of chemical evolution together with the physics involved in the formation and evolution of galaxies (Cora 2006; Lagos, Cora & Padilla 2008; Tecce et al. 2010).

This work is organized as follows. In Section 2, we present the model of galaxy formation used that combines a cosmological dark-matter only simulation and the semi-analytic model of galaxy formation SAG, giving a brief description of the latter with emphasis on the formation of elliptical galaxies, the chemical aspects and the new implementation of extended bursts of star formation (Subsection 2.2); Subsection 2.3 is devoted to the detailed description of the implementation of the TH-IGIMF. In Section 3, we present a summary of the calibration process involved in this work and show the first results of the  $[\alpha/\text{Fe}]$ -stellar mass relation with a universal Salpeter IMF (3.2). In Section 4, we analyse the impact of a variable IMF on the development of the  $[\alpha/\text{Fe}]$ -stellar mass relation, discussing the influence of the various time-scales involved in the modelling of formation of elliptical galaxies, such as starburst timescales and SNe delay times (Subsection 4.2). In Subsection 4.3 we test the implementation of the variable IMF by means of the resultant luminosity functions and mass-to-light ratios. In Section 5 we study in detail the global formation timescales of galaxies and analyze their impact on the development of the  $[\alpha/\text{Fe}]$ -stellar mass relation and the existence of a downsizing pattern. In Section 6, we mention previous investigations in the field putting in context our own results, with the perspective of future research work related to the main topic of this paper. We present our conclusion in Section 7. Finally, we add complementary information in appendix A, where we detail the physical recipes implemented in the model and the link with the free parameters involved in the calibration procedure that allows to obtain the best-fitting values.

## 2 MODEL OF GALAXY FORMATION

In the present work, we use a model of galaxy formation that combines a dissipationless cosmological  $N$ -body simulation with a semi-analytic model of galaxy formation and evolution. In the following, we describe the features of the simulation used and those aspects of the semi-analytic code that are relevant for the present study.

### 2.1 $N$ -body simulation

The DM only  $N$ -body simulation used for this study considers the standard  $\Lambda$ -CDM scenario, characterized by cosmological parameters  $\Omega_m = 0.28$ ,  $\Omega_b = 0.046$ ,  $\Omega_\Lambda = 0.72$ ,  $h = 0.7$ ,  $n = 0.96$ ,  $\sigma_8 = 0.82$ , according to the WMAP7 cosmology (Jarosik et al. 2011). The simulation was run with GADGET-2 (Springel 2005) using  $640^3$  particles in a cubic box of comoving sidelength  $L = 150 h^{-1} \text{Mpc}$ . The initial conditions were generated using GRAFIC2 (Bertschinger 2001). The simulation was evolved from  $z_{\text{ini}} = 61.2$  to the present epoch, storing 100 outputs equally spaced in  $\log_{10}(a)$  between  $z = 20$  and  $z = 0$  (Benson et al. 2012).

DM haloes were identified using a friends-of-friends (FOF) algorithm. Then, the application of SUBFIND algorithm (Springel et al. 2001) allows to select self-bound substructures (subhaloes) having at least 10 particles, with a mass of  $1 \times$

$10^9 h^{-1} \text{M}_\odot$  each. DM haloes and subhaloes have masses in the range  $1 \times 10^{10} - 7.8 \times 10^{14} h^{-1} \text{M}_\odot$ .

### 2.2 Semi-analytic model of galaxy formation

We use the semi-analytic model SAG described in the works of Cora (2006), Lagos et al. (2008) and Tecce et al. (2010), which is based on the version of the Munich semi-analytic model presented by Springel et al. (2001). In this section, we describe briefly the main features of the model, giving more details of aspects closely related with the aim of this research work, that is, the chemical implementation and the channels of bulge formation that give rise to the population of elliptical galaxies. The time-scales involved in the formation of this stellar component are crucial in the understanding of the development of the  $[\alpha/\text{Fe}]$ -stellar mass relation. Several modifications have to be included for a proper treatment of this aspect, which are also described in detail.

#### 2.2.1 Main features of SAG

The semi-analytic model SAG uses the subhalo merger trees provided by the underlying simulation to generate the galaxy population. Cold gas is settled in the centres of DM subhaloes as a result of the radiative cooling suffered by the hot gas contained within them. It is assumed that the cold gas disc has an exponential density profile (Tecce et al. 2010). When the density of cold gas becomes high enough, SF in the disc is triggered according to the conditions given by Croton et al. (2006) which are considered in the current version of SAG. We refer to this mode of SF as quiescent SF. One aspect that changed with respect to previous versions of SAG is the estimation of the gas cooling rate; we now consider the total radiated power per chemical element given by Foster et al. (2012)<sup>1</sup>. The only galaxies for which inflow of cooling gas from the intergalactic medium takes place are central galaxies. These galaxies, also named *type 0*, reside within the most massive subhalo within a FOF halo. Satellite galaxies are classified in two types, those residing in smaller subhaloes of the same FOF halo (*type 1*), and those which DM subhalo are below the resolution limit as a result of mass loss caused by tidal forces (*type 2*). Galaxies of the latter type merge with the central galaxy of their host subhalo after a dynamical friction time-scale (Binney & Tremaine 2008). When a galaxy becomes a satellite of either type, it suffers strangulation, that is, all of its hot gas halo is removed and transferred to the hot gas component of the corresponding type 0 galaxy. From a given star formation event and an IMF adopted, we can estimate the number of SNe CC that contribute to energy feedback. Effects of feedback from active galactic nuclei (AGN) are also included (Lagos et al. 2008). The energy injection from both sources regulates the star formation through the transfer of gas and metals from the cold to the hot gas phase.

#### 2.2.2 Formation of elliptical galaxies

The morphological classification of galaxies generated by the model is based on the ratio between bulge and total  $r$ -band luminosity, B/T. Elliptical galaxies are those characterized by a ratio  $B/T > (B/T)_{\text{thresh}}$ , where the parameter  $(B/T)_{\text{thresh}}$  may adopt

<sup>1</sup> These modifications were already taken into account in the version of SAG considered to evaluate the capability of the calibration method used to tune the free parameters of the model (Ruiz et al. 2014).

values in the range  $\sim 0.7 - 0.85$ . Thus, the formation of elliptical galaxies is directly connected with bulge formation, which in SAG takes place through global disk instabilities and two different kinds of galactic mergers.

When a galaxy merger occurs, the stellar mass ratio between the satellite galaxy and the central galaxy,  $M_{\text{sat}}/M_{\text{cen}}$ , is evaluated. If  $M_{\text{sat}}/M_{\text{cen}} > 0.3$ , then the merger is considered as a major one. In this case, all the gas in the remnant galaxy is consumed in a starburst contributing to the bulge formation, and the stellar disc is completely relaxed and transferred to the bulge. The triggering of a starburst in a minor merger ( $M_{\text{sat}}/M_{\text{cen}} \leq 0.3$ ) will depend on the fraction of cold gas present in the disc of the central galaxy, as implemented by Lagos et al. (2008) following the work of Malbon et al. (2007). If the ratio between the cold gas and the disc mass of the central galaxy,  $M_{\text{cold,cen}}/M_{\text{disc,cen}}$ , is larger than a fixed parameter  $f_{\text{burst}} = 0.6$ , then the perturbation introduced by the merging satellite drives all the cold gas from both galaxies into the bulge component, where it is consumed in a starburst; the disc mass is given by the sum of the cold gas and the stars formed through quiescent SF. However, if the satellite is much less massive than the central galaxy ( $M_{\text{sat}}/M_{\text{cen}} \leq 0.05$ ), no burst occurs. In minor mergers, only the stars of the merging satellite are transferred to the bulge component of the central galaxy.

The other channel that contributes to the bulge formation is the global disk instability. Some configurations of galactic discs do not remain stable with time. When a galactic disc is sufficiently massive that its self-gravity is dominant, it becomes unstable. This condition is expressed in the model through the Efstathiou-Lake-Negroponte (Efstathiou et al. 1982) criterium, that is, the stability to bar formation is lost when

$$\epsilon_d \equiv \frac{V_{\text{disc}}}{(GM_{\text{disc}}/R_{\text{disc}})^{1/2}} \leq \epsilon_{\text{thresh}}, \quad (1)$$

where  $M_{\text{disc}}$  is the mass of the disc (cold gas plus stars),  $R_{\text{disc}}$  is the disc scale radius, and  $V_{\text{disc}}$  is the circular velocity of the disc. For the latter, we use the velocity where the rotation curve flattens, which we approximate by the velocity calculated at  $\sim 3R_{\text{disc}}$  (see Tecce et al. (2010) for details concerning disc features). The free parameter  $\epsilon_{\text{thresh}}$  has values close to unity; in our model, we adopt  $\epsilon_{\text{thresh}} = 1$ . We consider an additional free parameter that takes into account the influence of a perturbing galaxy that effectively triggers the disc instability; this is modelled by computing the mean separation between galaxies in a FOF group. When the mean separation is smaller than  $f_{\text{pert}} R_{\text{disc}}$ , being  $f_{\text{pert}}$  a free parameter, we consider that a neighbouring galaxy perturbs the unstable disc. As a consequence of this, all the stars and cold gas in that disc are transferred to the bulge component, and all the gas present is consumed in a starburst.

### 2.2.3 Chemical enrichment model

In our chemical model, we follow the production of ten chemical elements (H,  $^4\text{He}$ ,  $^{12}\text{C}$ ,  $^{14}\text{N}$ ,  $^{16}\text{O}$ ,  $^{20}\text{Ne}$ ,  $^{24}\text{Mg}$ ,  $^{28}\text{Si}$ ,  $^{32}\text{S}$ ,  $^{40}\text{Ca}$ ) generated by stars in different mass ranges, from low- and intermediate-mass stars to quasi massive and massive stars. This version of SAG is characterized by a new set of stellar yields. We use the best combination of stellar yields reported by Romano et al. (2010), selected to be in accordance with the large number of constraints for the Milky Way. For low and intermediate-mass stars (LIMS), in the mass interval  $1 - 8M_{\odot}$ , we use the yields of Karakas (2010). For the mass loss of pre-supernova stars (He and CNO elements), we use the yields computed by the Geneva group (Hirschi et al.

2005), and for the yields of the explosive nucleosynthesis due to SNe CC, we use the results of Kobayashi et al. (2006). In all cases, we have adopted the total ejected mass of solar metallicity models, for which the solar abundances of Anders & Grevesse (1989) are assumed, with a solar composition  $Z_{\odot} = 0.02$ .

Ejecta from SNe Ia are also included, which are characterized by high iron production ( $\sim 0.6M_{\odot}$ ); we consider the nucleosynthesis prescriptions from the updated model W7 by Iwamoto et al. (1999). The SNe Ia rates are estimated using the single degenerate model, in which a SN Ia occurs by carbon deflagration in C-O white dwarfs in binary systems whose components have masses between  $0.8$  and  $8M_{\odot}$  (Greggio & Renzini 1983); we implement the formalism presented by Lia et al. (2002) (see their Section 4.2.2). The fraction of these binary systems,  $A_{\text{bin}}$ , is one of the free parameters of SAG. We take into account the return time-scale of mass losses and ejecta from all sources considered. For this purpose, we use the stellar lifetimes given by Padovani & Matteucci (1993) who use results from Matteucci & Greggio (1986) for masses over  $6.6M_{\odot}$ , and from Renzini & Buzzoni (1986) for masses below this limit. This aspect becomes especially relevant for this work because of the different delay times that characterize different types of SNe, which affect the abundance of  $\alpha$ -elements relative to iron. For a detailed description of the implementation in SAG of the chemical enrichment of the different baryonic components, we refer the reader to Cora (2006).

### 2.2.4 Extended starbursts

In previous versions of the model, the formation of stars in the bulge occurs through starbursts that consume the available cold gas in a single step<sup>2</sup>. We now consider that starbursts are characterized by a given time-scale during which the cold gas driven to the galactic center is consumed gradually in several steps. Thus, this cold gas has the possibility of being progressively contaminated by the stars formed in the bulge. This way, the  $[\alpha/\text{Fe}]$  abundance ratio of successive generations of stars in the bulge is not only determined by the abundances of the disc cold gas at the moment in which the starburst is triggered, but is also modified by the relative contribution of different types of SNe, which depends on the relation between the time-scale of the duration of the starburst and the lifetime of SNe progenitors.

The cold gas that will be eventually converted in bulge stars is referred to as bulge cold gas, in order to differentiate it from the disc cold gas. The amount of bulge cold gas available allows us to make a first estimation of the mass of stars that will be formed in the bulge. Then, we compute the time-scale in which they would form, which is chosen to be the dynamical time considered in quiescent SF as a first approximation, that is, the one defined as the ratio between the scale radius of the exponential profile that characterizes the galactic disc and its circular velocity. This choice seems reasonable since a burst normally takes place via a bar embedded in the galaxy disc. Thus, from the ratio of the bulge cold gas mass and the time-scale estimated for the duration of the starburst, we know the mass of stars that will be formed in each time step. For simplicity, SF throughout the extended starburst process occurs at a constant rate. Other works in the literature that have taken into account the starbursts time-scales consider that the SFR in a burst decays exponentially with time after the burst is triggered (Granato et al.

<sup>2</sup> Differential equations in SAG are integrated in time-steps of equal size used to subdivide the intervals between simulation outputs.

2000; Lacey et al. 2008). We justify our assumption considering that the bar formed during the instability, triggered either by a galaxy merger or a disk instability, favours the gradual feeding of the bulge cold gas reservoir by the disc cold gas that is being driven to the galactic center (e.g. Kormendy & Kennicutt 2004), keeping constant the conditions that give rise to SF. Note that the presence of a bar during the process of bulge formation is only implicit in the assumption of constant SFR during starbursts. Modelling bar formation is not an easy task (see Kormendy & Kennicutt 2004; Athanassoula 2013), and is beyond the scope of this paper.

### 2.3 Variable IMF

The stellar IMF has a great influence on the chemical enrichment of galaxies since it defines the amount of stars formed in each stellar mass interval for each star formation event and, consequently, impacts on the amount of metals returned to the ISM, where new stars will eventually form. The IMF also determines the number of SNe CC involved in the estimation of the reheated mass that is transferred from the cold to the hot phase during SN feedback. Today, there is some consensus that in a simple stellar population the slope of the IMF above  $1 M_{\odot}$  is not strictly different from that of Salpeter IMF ( $\alpha \equiv 1 + x = 2.35$ ); stars with masses over  $1 M_{\odot}$  are the major contributors to chemical enrichment (Chiosi et al. 1998). Several attempts have been made in measuring this important distribution function in the solar neighbourhood (Salpeter 1955; Chabrier 2003) or directly in star clusters (Kroupa 2001; Kroupa & Boily 2002). The latter is represented by a multi-component power-law IMF given by

$$\xi(m) = k \begin{cases} k' \left(\frac{m}{m_H}\right)^{-\alpha_0} & , m_{\text{low}} \leq m/M_{\odot} < m_H \\ \left(\frac{m}{m_H}\right)^{-\alpha_1} & , m_H \leq m/M_{\odot} < m_0, \\ \left(\frac{m_0}{m_H}\right)^{-\alpha_1} \left(\frac{m}{m_0}\right)^{-\alpha_2} & , m_0 \leq m/M_{\odot} < m_1, \\ \left(\frac{m_0}{m_H}\right)^{-\alpha_1} \left(\frac{m_1}{m_0}\right)^{-\alpha_2} \left(\frac{m}{m_1}\right)^{-\alpha_3} & , m_1 \leq m/M_{\odot} \leq m_{\text{max}}, \end{cases} \quad (2)$$

with  $m_{\text{low}} = 0.01$ ,  $m_H = 0.08$ ,  $m_0 = 0.5$  and  $m_1 = 1.0$ , and exponents  $\alpha_0 = 0.3$ ,  $\alpha_1 = 1.3$ ,  $\alpha_2 = \alpha_3 = 2.35$ . The normalization constant  $k$  contains the desired scaling of the IMF (for example, to the total mass of the system). Note that brown dwarfs are a separate population and contribute about 1.5 per cent by mass only. Therefore, they have a different normalisation factor,  $k'$  ( $k' \sim 1/3$ , Thies & Kroupa 2007, 2008). In the case of stellar systems with composite stellar populations, other aspects must be considered.

A galaxy-wide IMF may be represented by an integrated galactic initial mass function (IGIMF) proposed by Kroupa & Weidner (2003), whose theory was developed in the last decade (see Kroupa et al. 2013, for a review). This formalism states that star formation takes place exclusively in star clusters (Lada & Lada 2003). This way, the stellar populations of each galaxy are composed by stars in surviving and dissolved star clusters. Within each star cluster, stars form with the stellar IMF given by eq. 2. The embedded star clusters in the galaxy also follow an initial distribution of masses of the form  $\xi_{\text{ecl}}(M_{\text{ecl}}) dM_{\text{ecl}} \propto M_{\text{ecl}}^{-\beta} dM_{\text{ecl}}$ , where  $M_{\text{ecl}}$  is the mass of the embedded star cluster. Moreover, the most massive star in a cluster,  $m_{\text{max}}$ , is related in a non-trivial way with the cluster mass (Weidner et al. 2013); the mass of the most massive star is higher in more massive clusters. Furthermore, observations indicate that higher SFRs lead to the formation of brighter clusters (Larsen 2002). Weidner et al. (2004)

find that this empirical correlation can be transformed into a relation between the SFR of the galaxy and the maximum embedded cluster mass of the form

$$M_{\text{ecl}}^{\text{max}}(\text{SFR}) = 8.5 \times 10^4 \text{ SFR}^{0.75} M_{\odot}. \quad (3)$$

The IGIMF is the sum of all the new born stars in all of the star clusters considering the above ingredients, that is,

$$\xi_{\text{IGIMF}}(m, t) = \int_{M_{\text{ecl}}^{\text{min}}}^{M_{\text{ecl}}^{\text{max}}(\text{SFR}(t))} \xi(m \leq m_{\text{max}}(M_{\text{ecl}})) \xi_{\text{ecl}}(M_{\text{ecl}}) dM_{\text{ecl}}, \quad (4)$$

where  $\xi(m \leq m_{\text{max}}(M_{\text{ecl}}))$  is the stellar IMF given by eq. 2, and  $M_{\text{ecl}}^{\text{min}}$  defines the minimum mass of cluster that can be formed in a galaxy, which is a free parameter of the IGIMF model. Now, for this formulation of the IGIMF, it is assumed that star formation in all the star clusters at all epochs is produced with a canonical IMF. However, violent star formation conditions could drive crowding in massive star clusters (Elmegreen 2004; Shadmehri 2004), and the formation of massive stars could be favoured under such conditions, given that the low-mass limit of star formation would be higher. Following preliminary work of Marks et al. (2012), Weidner et al. (2011, WKP11 hereafter) consider that, for embedded clusters  $M_{\text{ecl}} < 2 \times 10^5 M_{\odot}$ , the slope of the canonical IMF (eq. 2) for stars more massive than  $1.3 M_{\odot}$  is  $\alpha_3 = 2.35$ . For larger cluster masses, the dependence of the stellar IMF slope for stars in this mass range is given by

$$\alpha_3(M_{\text{ecl}}) = -1.67 \times \log_{10} \left( \frac{M_{\text{ecl}}}{10^6 M_{\odot}} \right) + 1.05, \quad (5)$$

The effect of this assumption in the IGIMF is analysed in WKP11. The high-mass end of the IGIMF is, in general, steeper than the stellar IMF since the formation of low mass stars is favoured. However, if one includes the effect of crowding in massive clusters, as we have seen, the slope of the canonical IMF for massive stars can become more top heavy than the Salpeter IMF for these massive clusters. When a starburst event with high SFR occurs in a galaxy, the formation of massive clusters is favoured and the formation of massive stars is highly enhanced, so the IGIMF can become also more top heavy than the Salpeter IMF for high mass stars.

This formulation leads to the top heavy IGIMF (TH-IGIMF; WKP11). The slope of this TH-IGIMF above  $1.3 M_{\odot}$  can then be computed by a least-squares fit to the calculated IGIMF. Hence, the TH-IGIMF can be translated into a power law of a form similar to the canonical stellar IMF used to derive the IGIMF, but with an exponent  $\alpha_{\text{TH}}$  for high mass stars, that is,

$$\xi_{\text{TH}}(m) = k \begin{cases} \left(\frac{m}{m_H}\right)^{-\alpha_1} & , m_H \leq \frac{m}{M_{\odot}} < m_0, \\ \left(\frac{m_0}{m_H}\right)^{-\alpha_1} \left(\frac{m}{m_0}\right)^{-\alpha_2} & , m_0 \leq \frac{m}{M_{\odot}} < m_1, \\ \left(\frac{m_0}{m_H}\right)^{-\alpha_1} \left(\frac{m_1}{m_0}\right)^{-\alpha_2} \left(\frac{m}{m_1}\right)^{-\alpha_{\text{TH}}} & , m_1 \leq \frac{m}{M_{\odot}} \leq m_{\text{max}}. \end{cases} \quad (6)$$

where  $m_H = 0.1$ ,  $m_0 = 0.5$  and  $m_1 = 1.3$ .

After having introduced the basic aspects of the TH-IGIMF theory, we describe the way in which it is implemented in SAG. Although the reference to “starbursts condition” in the work of WKP11 implies a high level of star formation rate in a starburst, we use the resulting dependence of the  $\alpha_{\text{TH}}$  with SFR for any event of star formation in our model, that is, without making any distinction between quiescent star formation mode and starbursts. For each star formation event, we assign to it the TH-IGIMF given by eq. 6, according to the corresponding SFR. The model considers small variations of  $\log(\text{SFR})$  so that the slope of the TH-IGIMF is

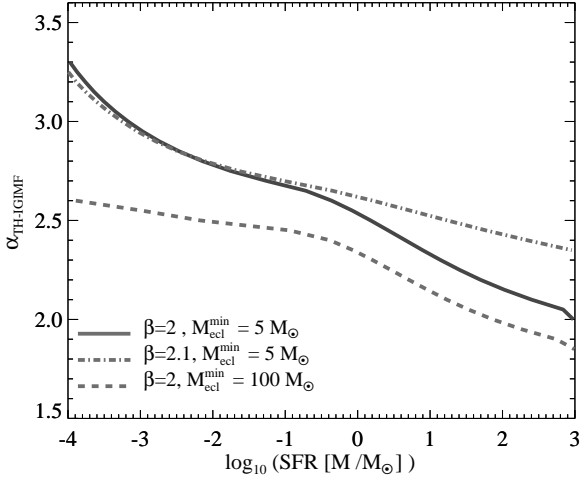


**Figure 1.** Dependence of the slope of the TH-IGIMF ( $\alpha_{\text{TH}}$ ) on the SFR for different minimum embedded cluster masses and slopes of the embedded star cluster mass function: (i)  $\beta = 2$ ,  $M_{\text{ecl}}^{\text{min}} = 5 M_{\odot}$  (solid line), (ii)  $\beta = 2.1$ ,  $M_{\text{ecl}}^{\text{min}} = 5 M_{\odot}$  (dashed-dotted line), and (iii)  $\beta = 2$ ,  $M_{\text{ecl}}^{\text{min}} = 100 M_{\odot}$  (dashed line).

binned in steps of 0.05. We adopt  $m_{\text{H}} = 0.1 M_{\odot}$  for the lower limit in the TH-IGIMF according to our chemical implementation.

We consider embedded cluster mass functions characterized by different values of the exponent  $\beta$ , and of the minimum embedded cluster masses  $M_{\text{ecl}}^{\text{min}}$ . We explore cases with (i)  $\beta = 2$  and  $M_{\text{ecl}}^{\text{min}} = 5 M_{\odot}$ , (ii)  $\beta = 2.1$  and  $M_{\text{ecl}}^{\text{min}} = 5 M_{\odot}$ , and (iii)  $\beta = 2$  and  $M_{\text{ecl}}^{\text{min}} = 100 M_{\odot}$ . It is worth noting that some stellar associations with masses as low as  $5 M_{\odot}$  are found in the galaxy (e.g. Taurus-Auriga star-forming regions, Kirk & Myers 2011), thus favouring the lowest value of  $M_{\text{ecl}}^{\text{min}}$  considered here. Therefore, at least in quiescent star forming conditions, the  $M_{\text{ecl}}^{\text{min}}$  is supported observationally. However, this constraint could not be valid in more extreme star-forming conditions.

Fig. 1 shows the slope  $\alpha_{\text{TH}}$  as a function of the SFR for different values of  $M_{\text{ecl}}^{\text{min}}$  and  $\beta$ . It is clear from this plot that the slope  $\alpha_{\text{TH}}$  of the TH-IGIMF is larger than the slope of the Salpeter IMF (characterized by a fixed value of  $\alpha$  for all SFR) in lower star formation regimes. The values of SFR at which the TH-IGIMF becomes more top heavy than Salpeter depend on the value of  $\beta$  and  $M_{\text{ecl}}^{\text{min}}$ , being of the order of 1, 10 and  $1000 M_{\odot} \text{ yr}^{-1}$  for  $\beta = 2$  and  $M_{\text{ecl}}^{\text{min}} = 100 M_{\odot}$ ,  $\beta = 2$  and  $M_{\text{ecl}}^{\text{min}} = 5 M_{\odot}$ , and  $\beta = 2.1$  and  $M_{\text{ecl}}^{\text{min}} = 5 M_{\odot}$ , respectively.

During periods of high star formation activity, the formation of massive stars is favoured. For higher SFRs, the number of high mass stars in a TH-IGIMF becomes larger than in the Salpeter IMF, with the corresponding reduction of the number of low mass stars required by the IMF normalization. This aspect is crucial to understand the build-up of the  $[\alpha/\text{Fe}]$ -stellar mass relation, as we will see in Subsection 4.

### 3 CALIBRATION OF THE MODEL AND RESULTS FOR SALPETER IMF

The semi-analytic modelling involves the tuning of the free parameters through their calibration against a set of observations. For

this purpose, we use the Particle Swarm Optimization technique (Kennedy & Eberhart 1995) applied to our semi-analytic model SAG. The detailed description of the method is given in Ruiz et al. (2014). This procedure involves the variation of a selected set of free parameters of the model within a given range. With this novel method, we can explore a large parameter space and find the best global maximum of the likelihood surface. The free parameters that are tuned are associated to the modelling of the main physical processes included in the code, summarized in Appendix A. They are the efficiency of SF ( $\alpha$ ), the SNe feedback efficiency associated to the SF taking place in the disc ( $\epsilon$ ) and in the bulge ( $\epsilon_{\text{bulge}}$ ), the parameters related to the central supermassive black hole growth ( $f_{\text{BH}}$ ) and AGN feedback efficiency ( $\kappa_{\text{AGN}}$ ), the parameter involved in the triggering of disc instabilities ( $f_{\text{pert}}$ ), and the fraction of binary stars ( $A_{\text{bin}}$ ).

#### 3.1 Observational constraints

We evaluate the behaviour of the model considering two sets of observational constraints to calibrate the free parameters. The first set involves the  $z = 0$  luminosity function in the  $r$ -band ( $r$ -band LF), the relation between the mass of the central supermassive black hole and the bulge mass (BHB relation), and the redshift evolution of SNe Ia and SN CC rates. The second set also includes the  $[\alpha/\text{Fe}]$ -stellar mass relation of elliptical galaxies.

The LF is a fundamental constraint for semi-analytic models of galaxy formation, since it reflects the influence of SF and feedback processes. The low mass end of the LF is mainly associated to SNe feedback. This aspect is relevant to our work, since the different IMFs contribute with different numbers of SNe CC, being low (high) for IMFs with large (small) values of their slopes, and the feedback efficiency parameters,  $\epsilon$  and  $\epsilon_{\text{bulge}}$  must be properly tuned in order to produce results that do not underestimate (overestimate) the effect of SN feedback. On the other hand, the high knee and the drop in the high mass end of the LF of galaxies is mainly determined by AGN feedback. This process is thought to be responsible for quenching the SF in massive galaxies, contributing to the downsizing behaviour of galaxies. AGN feedback is also constrained through the BHB relation, since the central supermassive black hole is responsible for this process. Constraining the mass of bulges in galaxies through the BHB relation helps to obtain an adequate mixture of galaxy morphologies.

The evolution of the rates of SNe Ia and CC are particularly important in this study, since the number of different types of SNe and their corresponding yields have direct impact on the the  $[\alpha/\text{Fe}]$  abundance ratio of stars. The evolution of SNe CC rate not only determines the amount of  $\alpha$ -elements produced along the galaxy lifetime, but constitutes an alternative diagnostic of the evolution of the SFR given the short lifetime of the progenitors of SNe CC. Reproducing the observed SFR is a required condition for any of our models, but is particularly relevant for those involving a TH-IGIMF because of the dependence of its slope on the SFR. In turn, the slope of the TH-IGIMF determines the number of SNe CC and, consequently, the SNe feedback that contributes to regulate the star formation process. One of the calibration parameters,  $A_{\text{bin}}$ , determines the amount of binary systems that explode as SNe Ia, and therefore, the amount of iron recycled into the ISM that will be available during the formation of future generations of stars. Thus, it is crucial to constrain its value to avoid making wrong conclusions with respect to the  $[\alpha/\text{Fe}]$  abundance ratio in stars. We will resume the analysis of the SNe time-scales and the impact of the

**Table 1.** Values of the free parameters of models with Salpeter IMF: SAGS-c1 and SAGS-c2. SAGS-c1 is calibrated using the LFs in the r-band, the BHB-Mass relation and SNe rates as a function of redshift as observational constraints. For model SAGS-c2 we add the  $[\alpha/\text{Fe}]$ -mass relation to the set of constraints.

	Salpeter IMF	Salpeter IMF
Param	SAGS-c1	SAGS-c2
$\alpha_{\text{SF}}$	0.1271	0.2328
$\epsilon$	0.2263	0.2541
$\epsilon_{\text{bulge}}$	0.0513	0.0778
$\text{frac}_{\text{BH}}$	0.0139	0.0141
$k_{\text{AGN}}$	$2.32 \times 10^{-5}$	$4.34 \times 10^{-4}$
$A_{\text{bin}}$	0.0341	0.0383
$f_{\text{pert}}$	44.62	47.63

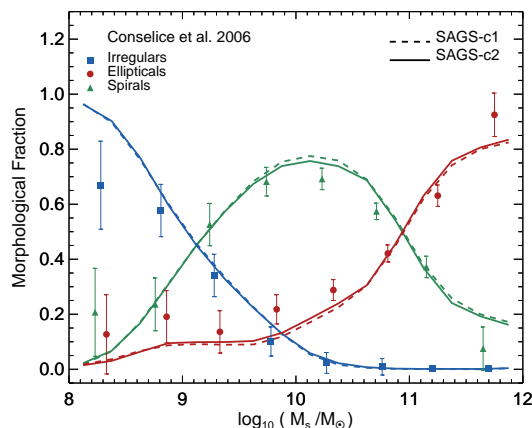


**Figure 2.** Fraction of galaxies of different morphological types as a function of the stellar mass for models SAGS-c1 (dashed line) and SAGS-c2 (solid line) compared with the observed morphological mixture in local galaxies (Conselice 2006). Irregular, spiral and elliptical galaxies in the model are represented by different colours, while the corresponding fractions inferred from observations are represented by triangles, rhombi and circles with the same colour code, as indicated in the key. Elliptical galaxies in the model are those satisfying the condition  $B/T > (B/T)_{\text{thresh}} \equiv 0.8$ .

parameter  $A_{\text{bin}}$  on the delay time-scales of SNe Ia when analysing the model with TH-IGIMF in Subsection 4.2.2.

It is important to note that SAG makes use of the luminosities of single stellar populations obtained with stellar population synthesis models, for which we use models by Bruzual & Charlot (2003) and Bruzual (2007). Since these models have an explicit dependence on the adopted IMF, they were generated for all the possible slopes of the TH-IGIMF of interest in this work. The unpublished 2007 models include the final prescription of Marigo & Girardi (2007) and Marigo et al. (2008) for the evolution of thermally pulsating-asymptotic giant branch (TP-AGB) stars. This produces significantly redder near-IR colors, and hence younger ages and lower masses, for young and intermediate-age stellar populations, than their 2003 counterpart; see Bruzual (2007) for details.

The observational data used for both sets of constraints are the r-band LF of Blanton et al. (2005), the BHB relation given by Häring & Rix (2004) and Sani et al. (2010), and the compilation of rates for both SNe Ia and SNe CC given by Melinder et al. (2012). In the second set of constraints, we also consider the  $[\alpha/\text{Fe}]$  ratio of elliptical galaxies presented in Thomas et al. (2010, T10 hereafter).

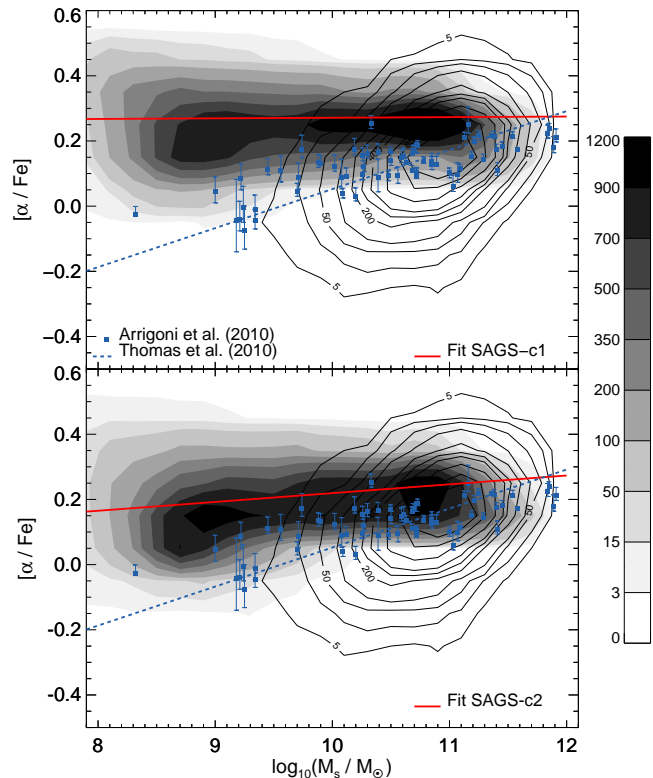


**Figure 3.**  $[\alpha/\text{Fe}]$ -stellar mass relation for elliptical galaxies in versions of SAG with Salpeter IMF: SAGS-c1 (top panel) and SAGS-c2 (bottom panel). The distributions of abundance ratios are represented by grey density contours; the red solid lines are the corresponding linear fits. Blue line contours depict the relation traced by the T10 sample of elliptical galaxies; the fit to the mean values of their  $[\alpha/\text{Fe}]$  abundance ratios for bins of stellar mass is represented by the blue dashed line. Blue symbols correspond to data from Arrigoni et al. (2010).

They analyse a subsample of 3360 galaxies out of 16502 early-type galaxies drawn from the Sloan Digital Sky Survey (SDSS) Data Release 4 (Colaboration 2006, DR4), and morphologically selected by visual inspection. The subsample is selected in the redshift range  $0.05 < z < 0.06$  to avoid biases in velocity dispersion. They obtain the  $[\alpha/\text{Fe}]$  abundance ratios for each galaxy in their sample by means of observed Lick spectral indices and stellar population synthesis models that take into account element abundance ratio effects. They also compute the dynamical mass of each galaxy from the line-of-sight stellar velocity dispersion using the scaling relation presented in Cappellari et al. (2006). This dynamical mass is considered a good proxy of the baryonic mass of elliptical galaxies, so we can compare the  $[\alpha/\text{Fe}]$ -stellar mass relation obtained from our model with the  $[\alpha/\text{Fe}]$ -dynamical mass relation presented by T10. The average errors of the observed  $[\alpha/\text{Fe}]$  values are of the order of 0.06 dex. We also consider the observational data set from Arrigoni et al. (2010), which was obtained by Trager et al. (2000) and re-analysed with the stellar population synthesis model described in Trager et al. (2008).



### 3.2 $[\alpha/\text{Fe}]$ -mass relation for a Salpeter IMF

The aim of this paper is to identify the main aspects involved in the build-up of the  $[\alpha/\text{Fe}]$ -stellar mass relation of elliptical galaxies. Our semi-analytic model provides the information needed to construct this relation. We classify a galaxy as early-type if the galactic bulge represents more than 80 per cent of the total baryonic mass of the galaxy, that is, we adopt  $(B/T)_{\text{thresh}} = 0.8$ . (see Subsection 2.2.2). With this criterion, we estimate the fraction of early-type and late type galaxies. Bulgeless galaxies are considered as irregulars.

Once we have selected the population of early-type galaxies in the model, we estimate the abundance ratio  $[\alpha/\text{Fe}]$  of their stellar component. Following Geisler et al. (2007), we define the  $[\alpha/\text{Fe}]$  abundance ratio as

$$[\alpha/\text{Fe}] = \frac{1}{6} \sum_{i=1}^6 [\alpha/\text{Fe}]_i, \quad (7)$$

where  $[\alpha/\text{Fe}]_i$  denotes the logarithm of the abundance ratio with respect to iron of each of the six  $\alpha$ -elements available in our chemical implementation ( $^{16}\text{O}$ ,  $^{20}\text{Ne}$ ,  $^{24}\text{Mg}$ ,  $^{28}\text{Si}$ ,  $^{32}\text{S}$ ,  $^{40}\text{Ca}$ ). For the sake of comparison with the observational data considered, we refer the abundance ratios of galaxies in the model to the solar abundances of Grevesse et al. (1996) as in T10 and Arrigoni et al. (2010).

We consider model SAG with Salpeter IMF and calibrate it using the two sets of observational constraints described in Section 3.1 giving place to two variants of the same model, referred to as SAGS-c1 and SAGS-c2. The inclusion of the  $[\alpha/\text{Fe}]$ -stellar mass relation as an additional constraint in the second set imposes more restrictions to the free parameters and their values change with respect to those obtained from the first set of constraints. The values of the parameters obtained for each calibration are presented in Table 1.

The fraction of galaxies with different morphological types for model SAGS-c1 and SAGS-c2 are presented in Figure 2. In both cases, they are in concordance with the observed fraction in the local Universe, for which we use data from Conselice (2006). The  $[\alpha/\text{Fe}]$ -stellar mass relation for the population of elliptical galaxies is shown in Figure 3 for both SAGS-c1 (top panel) and SAGS-c2 (bottom panel). Model results are compared with the  $[\alpha/\text{Fe}]$ -dynamical mass relation of elliptical galaxies given by T10 which is represented by blue line contours. The linear fit to this galaxy population is shown by the blue dashed line. The extrapolation of this fit to lower masses is in agreement with the trend denoted by data from Arrigoni et al. (2010), represented by blue squares.

We find that using only the  $r$ -band LF, the BHB relation and the evolution of the SN rates as constraints, the model is not able to reproduce the observed  $[\alpha/\text{Fe}]$ -stellar mass relation. In the galaxy population generated by SAGS-c1, less massive galaxies reach practically the same  $[\alpha/\text{Fe}]$  abundance ratios than more massive ones, giving rise to an  $[\alpha/\text{Fe}]$ -stellar mass relation with a flat trend, contrary to the observed one. This is reflected in the linear fit<sup>3</sup> to the distribution of the whole early type galaxy population represented by the red line. Grey coded contours depict the number of model elliptical galaxies.

Imposing the observed  $[\alpha/\text{Fe}]$ -stellar mass relation as an additional constraint allows to properly restrict the value of the SN feedback efficiency associated to the stars in the bulge ( $\epsilon_{\text{bulge}}$ ), and a positive correlation between  $[\alpha/\text{Fe}]$  abundances and stellar mass

is obtained from the model SAGS-c2, in better agreement with the observational trend. The larger value of  $\epsilon_{\text{bulge}}$  obtained from the second set of constraints favours the ejection of bulge cold gas in less massive galaxies. This gas reservoir may be later replenished for further star formation in the bulge with cold gas contaminated with higher iron abundances produced by the delayed contribution of SNe Ia. This change in  $\epsilon_{\text{bulge}}$  is complemented with a higher SF efficiency, which in turn demands a higher AGN feedback efficiency ( $k_{\text{AGN}}$ ) in order to achieve the right luminosities of high mass galaxies.

Although the slope of the  $[\alpha/\text{Fe}]$ -stellar mass relation for model SAGS-c2 is positive ( $a=0.025$ ) it is still almost flat; the slope of the fit to T10 data is  $a = 0.1184$ . This result highlights the difficulty of semi-analytic models to reproduce adequately this observed relation when using an universal IMF. Several groups have attempted to reproduce the slope of the  $[\alpha/\text{Fe}]$ -stellar mass relation using SAMs with a universal IMF during the last decade. Among the most recent ones, Arrigoni et al. (2010) find that with a top-heavier slope of the IMF, they can achieve a positive slope in the  $[\alpha/\text{Fe}]$ -stellar mass relation, close to the observed one. On the other hand, Calura & Menci (2009) use another SAM and show that simply changing the slope of the IMF seems to be insufficient to obtain the right slope in the observed relation. They argue that the assumption of a constant IMF flatter than Salpeter only lift the zero-point of the relation. We report here that when we change the slope of the IMF in SAG, we also have as a result a variation in the zero point, with no appreciable change in the slope, supporting the last conclusion. Calura & Menci (2011) include the effects of starbursts due to fly-by interactions at high redshift following the model developed by Cavaliere & Vittorini (2000) and studied by Menci et al. (2004) in their SAM. They find that the slope of the  $[\alpha/\text{Fe}]$ -stellar mass relation can be reproduced naturally when adding this effect, although the slope they obtain is shallower than expected from observations (see their Figure 1). The effect of starbursts triggered by companions is present in our model SAG through our particular implementation of disk instabilities (see Section 2.2.2). Forcing the free parameters of SAG to reproduce the  $[\alpha/\text{Fe}]$ -stellar mass relation with a Salpeter IMF gives a similar slope than the best model of Calura & Menci (2011), although in both cases the slope is too shallow compared with observations. Even constraining the parameters with the relation itself, it is not possible to achieve a satisfactory slope.

This procedure has shown the necessity of including the  $[\alpha/\text{Fe}]$ -stellar mass relation as a constraint. From now on, we will calibrate the versions of SAG with TH-IGIMF using the second set of constraints, and compare their results with those from model SAGS-c2, to which we will simply refer to as SAGS.

### 4 $[\alpha/\text{Fe}]$ -MASS RELATION: IMPACT OF A TH-IGIMF

The main aim of this work is to evaluate the impact of the variable TH-IGIMF on the development of the  $[\alpha/\text{Fe}]$ -mass relation in elliptical galaxies, motivated by the fact that a universal IMF is not able to reproduce the right slope of this relation even when the relation itself is used as a constraint. From the implementation of the TH-IGIMF in the updated version of SAG, we have the possibility to evaluate the impact of considering a variation of two different free parameters involved in the TH-IGIMF theory, that is, the minimum mass of the embedded star cluster and the slope of the embedded star cluster mass function (see section 2.3). Thus, we have three new different versions of SAG corresponding to i)  $M_{\text{ecl}}^{\text{min}} = 5M_{\odot}$ ,

<sup>3</sup> We use the IDL routine `robust_linefit.pro` ([http://idlastro.gsfc.nasa.gov/ftp/pro/robust/robust\\_linefit.pro](http://idlastro.gsfc.nasa.gov/ftp/pro/robust/robust_linefit.pro)).



**Table 2.** Calibration parameters for models SAGTH5B2, SAGTH5B21 and SAGTH100B2 which involve a TH-IGIMF characterized by a particular combination of the minimum embedded star cluster mass and the slope of the embedded star cluster mass function, that is, i)  $M_{\text{ecl}}^{\text{min}} = 5M_{\odot}$ ,  $\beta = 2$ , ii)  $M_{\text{ecl}}^{\text{min}} = 5M_{\odot}$ ,  $\beta = 2.1$  and iii)  $M_{\text{ecl}}^{\text{min}} = 100M_{\odot}$ ,  $\beta = 2$ , respectively.

TH-IGIMF			
Param	SAGTH5B2	SAGTH5B21	SAGTH100B2
$\alpha_{\text{SF}}$	0.0312	0.0338	0.0619
$\varepsilon$	0.3613	0.3532	0.2351
$\varepsilon_{\text{bulge}}$	0.3163	0.413	0.0479
$f_{\text{BH}}$	0.0516	0.0343	0.0765
$k_{\text{AGN}}$	$7.92 \times 10^{-5}$	$1.11 \times 10^{-4}$	$9.09 \times 10^{-5}$
$A_{\text{bin}}$	0.0386	0.04	0.0415
$f_{\text{pert}}$	39.96	48.36	34.08

$\beta = 2$ , ii)  $M_{\text{ecl}}^{\text{min}} = 5M_{\odot}$ ,  $\beta = 2.1$  and iii)  $M_{\text{ecl}}^{\text{min}} = 100M_{\odot}$ ,  $\beta = 2$ , to which we refer to as SAGTH5B2, SAGTH5B21 and SAGTH100B2, respectively.

#### 4.1 Impact of a TH-IGIMF

Testing new recipes to represent physical processes using a fixed set of free parameters is a common practice in semi-analytic modelling of galaxy formation. Generally, the preferred values of these parameters are kept for a modified version of the model in which some physical aspects are changed in order to evaluate the impact of the modifications introduced on the resulting galaxy properties. This is acceptable as long as the new version gives results in good agreement with the selected observational constraints. However, depending on the modifications introduced, this procedure might not be maintained.

Since the IMF has a strong impact on the results, each of the models with TH-IGIMF must be calibrated. Table 2 shows the values of the parameters adopted in the new calibrations, which include the  $[\alpha/\text{Fe}]$ -stellar mass relation as a constraint.

Fig. 4 shows the results of the abundance ratios  $[\alpha/\text{Fe}]$  of elliptical galaxies as a function of their stellar mass for models SAGTH5B2, SAGTH5B21 and SAGTH100B2 (left, middle and right panels, respectively); the corresponding galaxy distributions are shown in grey density contours. As mentioned in Subsection 3.2, elliptical galaxies in the model are those satisfying the condition  $B/T > (B/T)_{\text{thresh}} \equiv 0.8$ . With this criterion, the fraction of elliptical galaxies agree very well with the observed distribution in the three versions of the model after being calibrated. The  $[\alpha/\text{Fe}]$ -stellar mass distributions from our models are compared with the  $[\alpha/\text{Fe}]$ -dynamical mass relation presented by T10 (blue line contours) and data from Arrigoni et al. (2010) (blue squares). The blue dashed line denotes the linear fit to the  $[\alpha/\text{Fe}]$ -dynamical mass relation of T10, while the red solid line represents the linear fit to the distribution of model galaxies.

It is important to point out that the comparison of abundances ratios obtained from models that include a TH-IGIMF with the observed data considered here is not strictly fair. The final observed abundance patterns are obtained by comparing the observed spectral features of galaxies with synthetic spectra from stellar population synthesis models (SPSMs); these models assume a fixed stellar IMF that is not SFR dependent. The SPSMs models used by T10 are those of Thomas & Maraston (2003), who assume a Salpeter IMF to compute the parameters of the stellar populations. Arrigoni et al. (2010) use recomputed abundances from Trager et al. (2008), who also use the SPSMs corresponding to the

Salpeter IMF. Moreover, the observed abundance ratios are computed using integrated spectra of galaxies in a specific wavelength range. A fair comparison with model results should include luminosity weighted abundances in the corresponding bandwidth from our model. However, Thomas (1999) investigate the difference between luminosity and mass weighted abundances. They found that the difference is negligible in the case of a fixed IMF. Later on, Recchi et al. (2009) found that using an IGIMF, the difference between mass weighted and luminosity weighted abundances remain of the order of 0.1 dex. In light of these results, we compare the observed data directly with the abundances of SAG, that take into account the total mass of chemical elements in stars.

Keeping these inconsistencies in mind, we now analyse the features of the  $[\alpha/\text{Fe}]$ -stellar mass relation that emerge from our semi-analytic model for different values of  $M_{\text{ecl}}^{\text{min}}$  and  $\beta$ . Considering the plots in Fig. 4, we see that the TH-IGIMF produces a positive change in the trend of  $[\alpha/\text{Fe}]$  abundance ratios with stellar mass (grey shaded contours and fits represented by red solid lines) with respect to the one obtained for SAGS which considers a Salpeter IMF (green dotted line). The SFR dependent IMF helps to recover the slope denoted by observational data. Although this is the case for all the values considered for the minimum embedded star cluster mass and slope of the embedded cluster mass function, the agreement with the observational trend is particularly good for  $M_{\text{ecl}}^{\text{min}} = 5M_{\odot}$  and  $\beta = 2$  (right panel). The slope of the fit to the  $[\alpha/\text{Fe}]$  abundance ratios given by SAGTH5B2 ( $a = 0.088$ ) is steeper than those obtained from models SAGTH5B21 and SAGTH100B2 ( $a = 0.0568$  and  $a = 0.044$ , respectively). The former is closer to the slope of the fit to T10 data ( $a = 0.1184$ ) which was obtained taking into account all the galaxies in the sample; the value of 0.1 given by T10 corresponds to their subsample of red galaxies. All the combinations of parameters of the TH-IGIMF yield slopes of the fit to the  $[\alpha/\text{Fe}]$  abundance ratios closer to the observed one, than SAGS, that yields a slope of  $a = 0.025$ . However, if we consider median values, corresponding to the darker shaded contours, the model shows an excess of  $[\alpha/\text{Fe}]$  for all galaxy masses. This is related with a lack of Fe in the galaxies in all of our models. The modification of the SNIa delay times in the chemical implementation, as done by Yates et al. (2013), could improve this particular issue. We defer this analysis to a future work.

Considering that  $M_{\text{ecl}}^{\text{min}}$  and  $\beta$  are free parameters of the TH-IGIMF theory, the results that emerge from the analysis of Fig. 4 support a value as small as  $5M_{\odot}$  and 2 for these quantities. As we mentioned in Subsection 2.3, there is evidence of star forming clouds with masses down to  $5M_{\odot}$  and the slope of the embedded star cluster mass function is observed to be close to 2 (Lada & Lada 2003). However, the value of this minimum mass might change with redshift, shifting to higher values due to more violent star forming conditions. Weidner et al. (2013) also find evidence that the power-law index  $\beta$  of the mass function of the embedded star cluster decreases with increasing SFR. However, up to now there is no observational constraint or physical model that help to determine a preferred variation in elliptical galaxies. In order to understand the way in which a TH-IGIMF operates helping to achieve the correct  $[\alpha/\text{Fe}]$  abundance ratios for galaxies of different masses, we analyse the evolution of the mean slope of the TH-IGIMF ( $\langle\alpha_{\text{TH}}\rangle$ , see eq. 6) weighted with the stellar mass formed in each event, which is characterized by a given SFR, for galaxies within different mass ranges; galaxies in each mass range are selected according to their stellar mass at  $z = 0$ . This is shown in Fig. 5 for models SAGTH5B2, SAGTH5B21 and SAGTH100B2 (left-hand, middle and right-hand panels, respectively). The general evolution-

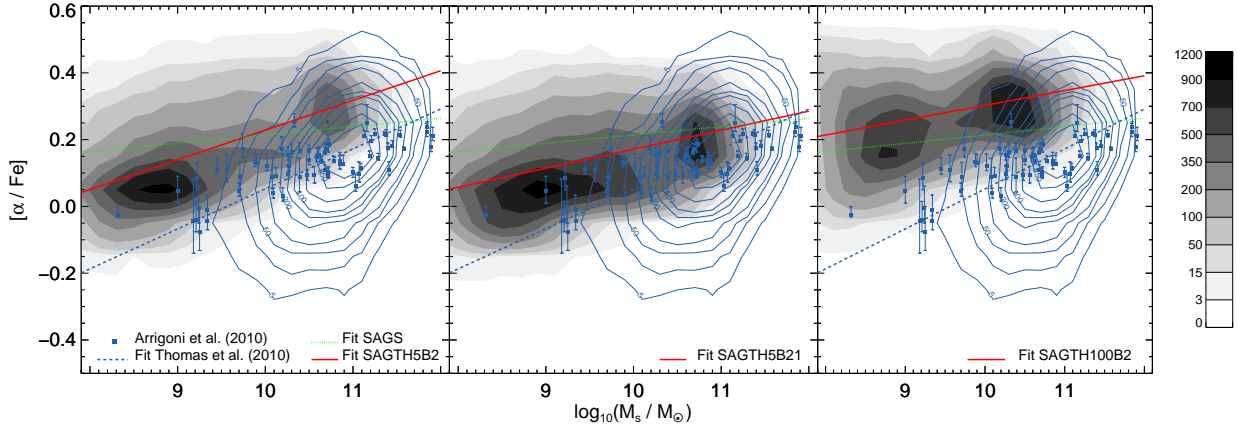


**Figure 4.**  $[\alpha/\text{Fe}]$ -stellar mass relation in models SAGTH5B2 (left panel), SAGTH5B21 (middle panel) and SAGTH100B21 (right panel) represented by grey density contours; the red solid lines are the fit to the distributions of abundance ratios. Results from all models are compared with the fit to the  $[\alpha/\text{Fe}]$ -stellar mass distribution of model SAGS, represented by a green dotted line. Blue line contours depict the relation traced by the T10 sample of elliptical galaxies; the fit to the observed distribution of  $[\alpha/\text{Fe}]$  abundance ratios vs. mass is represented by the blue dashed line. Blue symbols correspond to data from Arrigoni et al. (2010).

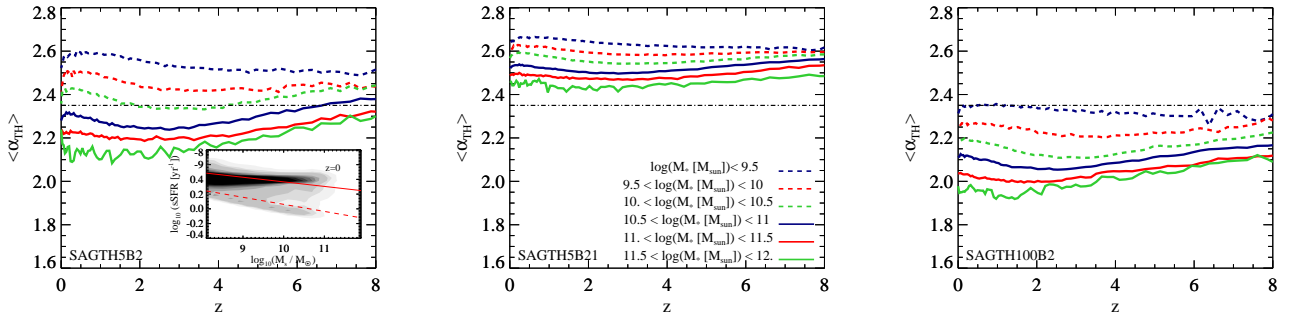


**Figure 5.** Evolution of the mean slope of the TH-IGIMF ( $\langle\alpha_{\text{TH}}\rangle$ , see eq. 6) weighted with the stellar mass formed in each event, which is characterized by a given SFR, for galaxies within different mass ranges, as indicated in the key; galaxies in each mass range are selected according to their stellar mass at  $z = 0$ . Results are shown for models SAGTH5B2 (left-hand panel), SAGTH5B21 (middle panel) and SAGTH100B2 (right-hand panel), characterized by the parameters  $M_{\text{ecl}}^{\text{min}} = 5M_{\odot}$  and  $\beta = 2$ ,  $M_{\text{ecl}}^{\text{min}} = 5M_{\odot}$  and  $\beta = 2.1$ , and  $M_{\text{ecl}}^{\text{min}} = 100M_{\odot}$  and  $\beta = 2$ , respectively. The horizontal dashed-dotted line in each panel represents the value of the slope of the Salpeter IMF. The inset in the left-hand panel contains the distribution of the specific star formation rate (sSFR) at  $z = 0$  as a function of stellar mass (grey shaded contours). The solid and dashed lines represent the linear fit to the sSFR distribution for active and passive galaxies, respectively; the limit between the two populations satisfy the condition defined by Kimm et al. (2011) (see their eq. 8).

any trend of  $\langle\alpha_{\text{TH}}\rangle$  is very similar for all models, but the values of  $\langle\alpha_{\text{TH}}\rangle$  for a given  $z = 0$  stellar mass range are lower for higher values of  $M_{\text{ecl}}^{\text{min}}$  and for lower values of  $\beta$ . Overall, regardless of the value of these free parameters, we can see that  $\langle\alpha_{\text{TH}}\rangle$  becomes progressively lower for more massive galaxies, that is, the star formation events taking place in more massive galaxies are characterized by flatter IMFs, which reflects that more massive galaxies have higher SFRs. These levels of star formation rate and their dependence with the stellar mass lead to adequate values of the specific SFR (sSFR), defined as SFR per unit stellar mass. This is shown in the inset panel in the plot on the left, where we can see that the sSFR at  $z = 0$  decreases with increasing stellar mass, in agreement with the general trend found by Feulner et al. (2005) for galaxies at higher redshifts.

The lowest values of the slope for each mass range are reached at earlier epochs for lower mass galaxies, shifting from  $1 \lesssim z \lesssim 2$  to  $3 \lesssim z \lesssim 4$ , for galaxies with  $z = 0$  stellar masses of  $\sim 5.6 \times 10^{11} M_{\odot}$  and  $\sim 1.8 \times 10^{10} M_{\odot}$ , respectively. The shape of the dependence of  $\langle\alpha_{\text{TH}}\rangle$  with redshift for each mass range indicates that lower mass progenitors have lower levels of SF and hence their star formation events are characterized by steeper IMFs. Thus, the progenitors of the most massive galaxies have a value of  $\langle\alpha_{\text{TH}}\rangle$  at  $z \approx 7$  quite similar to the corresponding value of galaxies within the mass range  $3.1 \times 10^{10} M_{\odot} < M_{\star} < 1 \times 10^{11} M_{\odot}$  at  $z \approx 3$ . It is interesting that the model SAGTH5B2, which gives a  $[\alpha/\text{Fe}]$ -stellar mass relation in better agreement with observations than the other two models (SAGTH5B21 and SAGTH100B2), has star formation events characterized by IMFs

steeper than the Salpeter IMF for low mass galaxies and top heavier for high mass galaxies, since the general discussion found in the literature considers that an IMF top-heavier than Salpeter IMF is needed to reproduce the observed  $[\alpha/\text{Fe}]$ -stellar mass relation (Nagashima et al. 2005; Calura & Menci 2009; Arrigoni et al. 2010). Calura & Menci (2009) propose that a top-heavy IMF should be considered when the SFR of the galaxies exceeds a value of  $100 \text{ M}_\odot \text{ yr}^{-1}$ . In that case, they obtain a positive slope of the  $[\alpha/\text{Fe}]$ - $\sigma$  relation, although the dependence becomes flat for galaxies with high velocity dispersion; when no starbursts triggered by interactions are taken into account, this dependence also becomes flat for low velocity dispersion galaxies (see their figure 20). The dichotomy in the dependence of the slope of the IMF with the SFR of the galaxy assumed in their model seems to prevent the development of a well behaved  $[\alpha/\text{Fe}]$ - $\sigma$  relation. The comparison of our results with those of Calura & Menci (2009) highlights the importance of a progressive and smooth variation of the slope in the IMF with the SFR supported by an empirically tested model of galaxy-wide IMF like the TH-IGIMF. From our investigation, we find that the key to achieve the correct dependence of  $[\alpha/\text{Fe}]$  abundance ratios with stellar mass is the combination of two aspects. On one hand, the difference of the IMF slope  $\langle\alpha_{\text{TH}}\rangle$  between galaxies with different masses, such that  $\langle\alpha_{\text{TH}}\rangle$  becomes progressively smaller for more massive galaxies. On the other, the values adopted by  $\langle\alpha_{\text{TH}}\rangle$ , which not only affect the slope of the  $[\alpha/\text{Fe}]$ -stellar mass relation but also its normalization.

Models with a TH-IGIMF characterized by higher values of  $M_{\text{ecl}}^{\text{min}}$  (SAGTH100B2) and a higher value of  $\beta$  (SAGTH5B21) give place to a  $[\alpha/\text{Fe}]$ -stellar mass relation with a positive slope since they also present relative differences in the values of  $\langle\alpha_{\text{TH}}\rangle$  for galaxies within different mass ranges, although these differences are smaller for the model with higher  $\beta$ . In the latter case, the values of  $\langle\alpha_{\text{TH}}\rangle$  are larger than that of Salpeter IMF regardless of the galaxy mass, while in model SAGTH100B2 the TH-IGIMF is always top-heavier than Salpeter IMF. In both cases, the  $[\alpha/\text{Fe}]$ -stellar mass relation is flatter than in SAGTH5B2. The fact that model SAGTH5B21 is characterized by TH-IGIMF steeper than Salpeter IMF also for massive galaxies makes these galaxies to be less enriched by  $\alpha$  elements that they should be, leading to a flatter  $[\alpha/\text{Fe}]$ -stellar mass relation. On the contrary, in model SAGTH100B2, virtually all star formation events contain a large number of massive stars above  $8 \text{ M}_\odot$ , thus displaying an enhanced production of SNe CC with the consequent over-abundance of  $\alpha$ -elements since galaxies of different mass have TH-IGIMF top-heavier than Salpeter IMF. These results point out in the direction that galaxies with masses smaller than  $\sim 3 \times 10^{10} \text{ M}_\odot$  should have IMF steeper than Salpeter IMF, while galaxies with higher masses should take top-heavier IMF than Salpeter IMF in order to achieve the right chemical abundances.

Our results allow to restrict the possible values of free parameters involved in the TH-IGIMF theory, that is, the minimum embedded star cluster mass and the slope of the embedded mass function, supporting a value as small as  $M_{\text{ecl}}^{\text{min}} = 5 \text{ M}_\odot$  for the former and of  $\beta = 2$  for the latter.

## 4.2 SNe delay times and extended bursts

In order to understand the particular pattern developed by the  $[\alpha/\text{Fe}]$  abundance ratios of elliptical galaxies, both the duration of the starbursts in galaxies within different mass ranges and the lifetime of progenitors of different types of SNe must be taken into

account.

### 4.2.1 Extended bursts and impact of different assumptions on the initial starburst duration

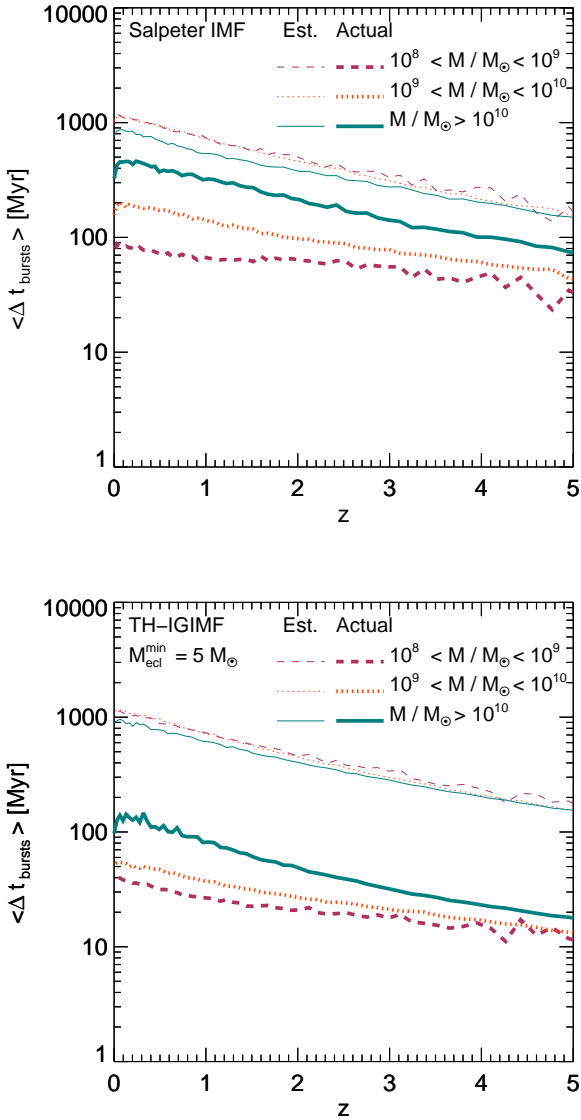
In section 2.2.4, we introduced the implementation of extended starbursts in SAG. We now analyze the results and their implications in the chemical evolution of elliptical galaxies. We also investigate the role of the extended bursts in the development of the  $[\alpha/\text{Fe}]$ -stellar mass relation.

Fig. 6 presents the mean duration of starbursts taking place in galaxies within different mass ranges as a function of redshift; galaxies are grouped according to their stellar mass at  $z = 0$ . The redshift indicates the time in which the starburst is triggered. We are considering here only starbursts that have ended as a result of the exhaustion of the bulge cold gas. There are several aspects to note in this plot. Firstly, the mean estimated time-scale of the starbursts (thin lines) increases with decreasing redshift, with a very similar trend for galaxies of different stellar mass. This arises because of the natural growth of galaxies that are characterized by larger dynamical times at more recent epochs. Secondly, the actual duration of the starbursts (thick lines) are shorter than the estimated burst time-scales for galaxies in all mass ranges. This is a result of the competition of several processes. The bulge cold gas reservoir is common to all the starbursts taking place simultaneously in a given galaxy. These starbursts may have been triggered at different times, contributing initially to increase the bulge cold gas reservoir. This reservoir is reduced by SNe feedback from stars in the bulge already formed in previous finished or on-going starbursts. The bulge cold gas is also reduced by the gradual growth of central BHs. These processes make starbursts reach their end before than originally estimated; this difference is more pronounced for less massive galaxies for which the cumulative effect of SNe feedback has stronger impact.

Considering starbursts triggered at  $z \approx 0$  in model SAGS (top panel), we find that their actual mean duration are of the order of  $9 \times 10^7 \text{ yr}$ ,  $2 \times 10^8 \text{ yr}$ , and  $5 \times 10^8 \text{ yr}$  for stellar masses within the ranges  $10^8 - 10^9 \text{ M}_\odot$ ,  $10^9 - 10^{10} \text{ M}_\odot$ , and larger than  $10^{10} \text{ M}_\odot$ , respectively. These values can be compared with the exponential time-scale of starbursts at  $z = 0$  given by the semi-analytic model used by Granato et al. (2000) (see their fig. 6), which is assumed to scale with the dynamical time-scale of the spheroid formed in a major merger; this process is the only channel of bulge formation that they consider. Their values of starburst time-scales range from  $5 \times 10^6 \text{ yr}$  to  $1 \times 10^8 \text{ yr}$  for galaxies within the mass range  $10^8 - 3 \times 10^{11} \text{ M}_\odot$ . The mean estimated duration of starbursts in model SAGS are of the same order of magnitude for all galaxies, being larger than the exponential time-scale of starbursts obtained by Granato et al. (2000).

The fact that, regardless of the redshift in which starbursts are triggered, the mean duration of the starbursts increase with stellar mass, contributes to explain the slightly positive slope in model SAGS. However, we emphasize here that the time-scale of galaxy formation, that is assumed to drive the relation of  $[\alpha/\text{Fe}]$  vs. mass in ellipticals by numerous works, is not linked to the duration of individual starbursts. The former is an integration over cosmic time of multiple star formation events.

This time-scale argument that explains the behaviour of the  $[\alpha/\text{Fe}]$ -stellar mass relation in the model is valid as long as we consider a universal IMF. A variable IMF which slope depends on the SFR gives different relative numbers of SNe Ia and SNe CC



**Figure 6.** *Top panel:* Mean duration of starbursts as a function of redshift for galaxies generated by model SAGS in different mass ranges, as indicated in the key; galaxies are grouped according to their stellar mass at  $z = 0$ . Mean estimated burst time-scales and actual duration of starbursts are represented by thin and thick lines, respectively. *Bottom panel:* Same as the top panel, but for model SAGTH5B2.

progenitors for each star formation event. This aspect plays an important role in the build-up of the  $[\alpha/\text{Fe}]$ -stellar mass relation, as we showed in Subsection 4.1. The dependence with redshift of starbursts in the case of the model SAGTHB2 (bottom panel of Fig. 6) is quite similar to the model with a Salpeter IMF, but the duration of the bursts are approximately a factor of two shorter.

The shorter duration of the starbursts in SAGTHB2 is explained by taking into account that the mean slopes of the IMF,  $\langle \alpha_{\text{TH}} \rangle$ , become progressively larger than the slope of the Salpeter IMF as we consider less massive galaxies (see left panel of Fig. 5). This fact leads to a low rate of SNe CC for low mass galaxies that have to be compensated by large values of the efficiency of SNe feedback for the disc and bulge ( $\epsilon$  and  $\epsilon_{\text{bulge}}$ , respectively), which are free

parameters of the model, in order to reproduce the faint end of the luminosity functions. These values are listed in Table 2; we can see that they are larger than the corresponding values for the calibrated model SAGS (Table 1), specially  $\epsilon_{\text{bulge}}$ .

Hence, galaxies in model SAGTH5B2 suffer, on average, a much stronger effect from SNe feedback arising from stars in the bulge than galaxies in model SAGS. This stronger effect contributes to deplete more rapidly the bulge cold gas reservoir for starbursts, reducing considerably their actual duration.

Contrary to what is obtained from model SAGS, the mean actual duration of starbursts given by model SAGTH5B2 and their dependence with the stellar mass are in good agreement with the exponential time-scale of starbursts at  $z = 0$  obtained by Granato et al. (2000), whose results are described above in this section. This good agreement is achieved from the consideration of a TH-IGIMF in our modelling. The values obtained from our model for the most massive galaxies are also consistent with results from numerical simulations given by Di Matteo et al. (2008), who find that the activity of merger-driven starbursts have a typical duration of a few  $10^8$  yr.

After having analysed the features of the estimated and actual mean duration of starbursts resulting from the modelling adopted in this work, we investigate the impact of a different assumption for the initial estimation of the starburst time-scale on the mean actual starburst duration and the  $[\alpha/\text{Fe}]$ -stellar mass relation. The combination of this quantity with the amount of bulge cold gas available defines its SFR. Thus, models of galaxy formation with a SFR dependent IMF, like the models with TH-IGIMF analysed here, will be affected by the choice of this initial value. SNe feedback and BH growth determine the actual duration of the starburst, but they keep the SFR unaltered.

We consider model SAGTH5B2 and modify the estimation of the initial duration of starbursts, adopting the simplest case in which all galaxies have the same initially estimated value for the duration of starbursts,  $\Delta t_{\text{burst}}^{\text{estimated}} = 50 \text{ Myr}$ . The mean estimated and actual duration of starbursts as a function of redshift for this modified model are shown in Fig. 7 for galaxies in different mass ranges. The thin line denotes the estimated value of starburst duration which is identical for all galaxies at all times. The mean actual values are characterized by redshift evolution which is pretty similar for all galaxies, and only show a very mild dependence with stellar mass at high redshifts. These values approach to the initially estimated ones as redshift decreases indicating that the potential well of galaxies become larger at lower redshifts with the consequent lower effect of SNe feedback. Since the initial estimated starburst time-scales are smaller than those estimated considering the disc dynamical time-scale (see lower panel of Fig. 6), the resulting actual starburst durations are also smaller.

Fig. 7 shows the impact of these shorter starbursts and their evolution on the  $[\alpha/\text{Fe}]$ -stellar mass relation obtained from the modified model SAGTH5B2. The red solid line denotes the linear fit to the distribution of  $[\alpha/\text{Fe}]$  abundance ratios with stellar mass. It has a slope of  $a = 0.076$ , a bit smaller than one corresponding to the model SAGTH5B2 that uses the dynamical time as an initial estimation of the starburst duration ( $a = 0.088$ ). Note that we are using the same set of parameters as those corresponding to the model SAGTH5B2.

All in all, different assumptions on the initial starburst duration do not produce a significant change on the pattern of chemical abundances of elliptical galaxies. These results provide additional support to our conclusions that the main responsible for the development of the proper trend of  $[\alpha/\text{Fe}]$  abundance ratios with

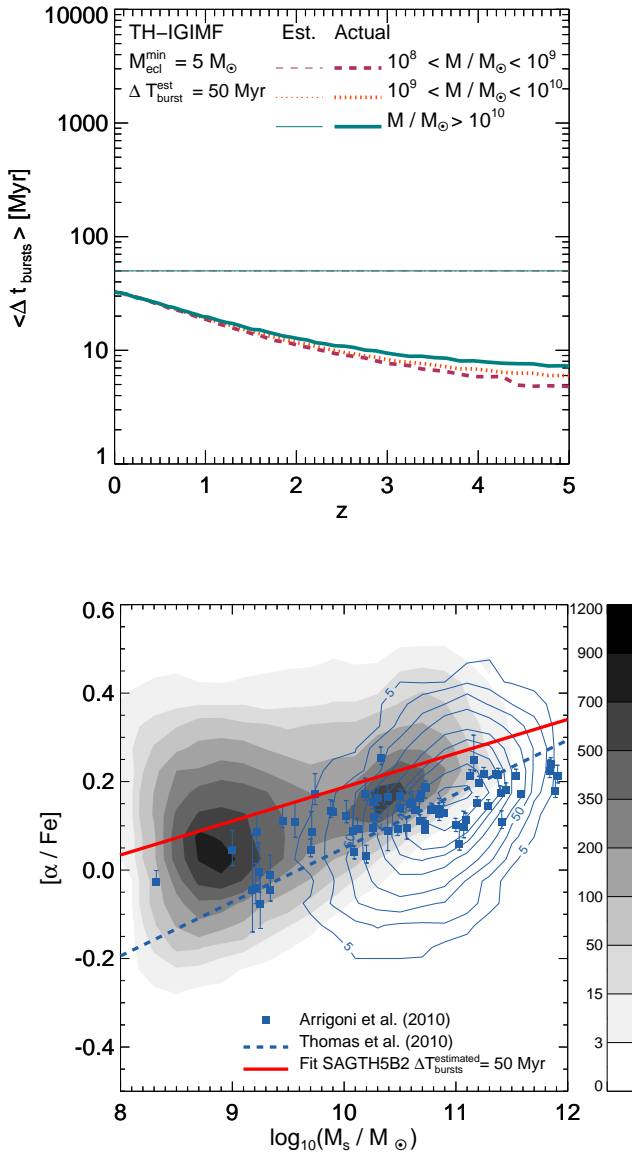


**Figure 7.** *Top panel:* Mean duration of finished starbursts as a function of the redshift in which they were triggered for galaxies in different mass ranges for model SAGTH5B2, as indicated in the key; galaxies are selected according to their stellar mass at  $z = 0$ . A fixed value of 50 Myr is assumed for the initial estimation of starburst time-scale of all galaxies. *Bottom panel:*  $[\alpha/\text{Fe}]$ -stellar mass relation for model SAGTH5B2 with a fixed initial value of estimated starburst timescale of 50 Myr for all galaxies.

stellar mass is a SFR dependent TH-IGIMF, being  $M_{\text{ecl}}^{\text{min}} = 5 M_\odot$  and  $\beta = 2$  the preferred values for the free parameters of this model.

#### 4.2.2 SNe delay times

The top panel of Fig. 8 shows the rates of SNe CC as a function of their delay times, that is, the time-scale for explosion. Different coloured lines correspond to the rates obtained from a TH-IGIMF with  $M_{\text{ecl}}^{\text{min}} = 5 M_\odot$  and  $\beta = 2$  and different possible values of  $\alpha_{\text{TH}}$ .

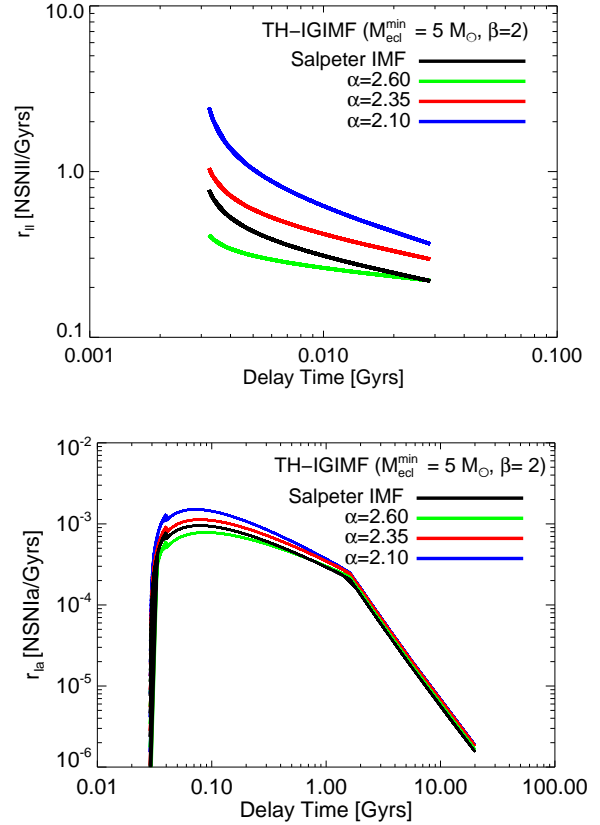


**Figure 8.** Rates of SNe CC and SN Ia as a function of their delay time for three different possible values of  $\alpha_{\text{TH}}$  for a TH-IGIMF with  $M_{\text{ecl}}^{\text{min}} = 5 M_\odot$  and  $\beta = 2$ .

As expected, flatter IMFs give place to larger SNe CC rates. These rates are compared with those obtained from a Salpeter IMF (black line). The SNe Ia rates corresponding to these four cases are presented in the bottom panel of Fig. 8.

As we mentioned in Section 2.2.3, the SNe Ia rate is estimated according to the formalism described in Lia et al. (2002) that assumes that SNe Ia originate in binary systems (Greggio & Renzini 1983). The fraction of these binary systems,  $A_{\text{bin}}$ , is one of the free parameters of SAG. For an assumed IMF, the value adopted by this parameter determines the SNe Ia rate. In the case of a universal IMF, like the Salpeter IMF adopted in model SAGS, the value of  $A_{\text{bin}}$  is linked to that IMF, constrained by the requirement of reproducing the observed evolution of SNe Ia rates. For a model with TH-IGIMF, the slope of the IMF for stellar masses larger than  $1.3 M_\odot$  (see eq. 6) can vary within a wide range, according to the SFR of a given star formation event. However, we consider a unique fraction of binary systems regardless of the slope of the IMF,  $\alpha_{\text{TH}}$ . Thus, SNe Ia rates for each single stellar population differ for different values of  $\alpha_{\text{TH}}$ , as can be seen in the bottom panel of Fig. 8, where the rates are given as a function of the SNe Ia delay times, which are set by the lifetime of the secondary star of the binary system. Lower (higher) values of  $\alpha_{\text{TH}}$  (flatter (steeper) IMF) determined by star formation events with higher (lower) SFR give place to lower (higher) SNe Ia rates. The value adopted by  $A_{\text{bin}}$  in the calibration process is the result of keeping the balance between the resulting SNe Ia rates from all the different possible values of  $\alpha_{\text{TH}}$  that can occur in all SF events in galaxies such that the average be-



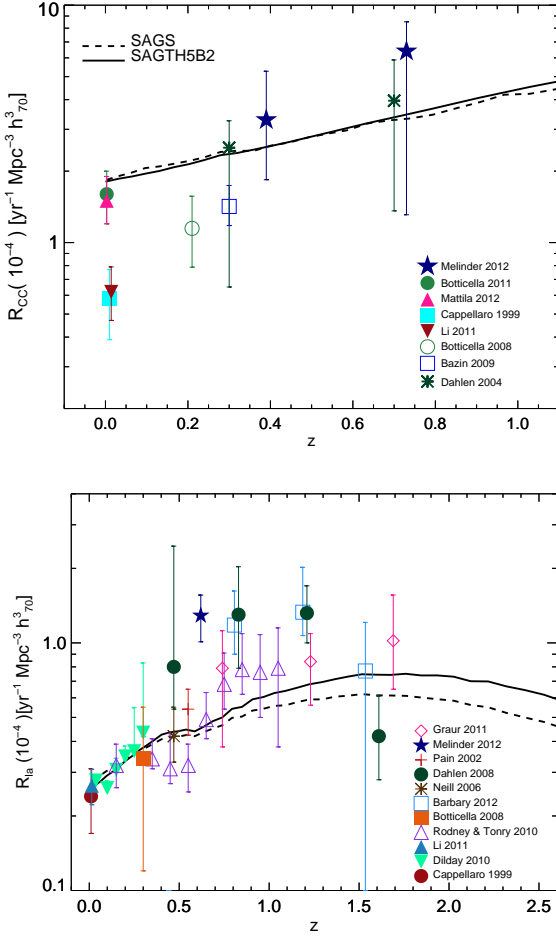


**Figure 9.** Evolution of SNe CC rates (top panel) and SNe Ia rates (bottom panel) given by models SAGS (dashed line) and SAGTH5B2 (solid line), compared with the compilation of observational determinations by Melinder et al. (2012).

haviour of the evolution of the SNe Ia rates for the whole galaxy population resembles the observed one.

Figure 9 shows the computed SNe rates as a function of redshift for both SAGS (dashed line) and SAGTH5B2 (solid line) models. The observational data corresponds to the compilation of Melinder et al. (2012). The evolution in the SNe CC rates are depicted in the top panel. Almost no difference arises between the results of the calibrated models SAGS and SAGTH5B2. The observed rates show a dichotomy at low redshift; while the works of Botticella et al. (2012) and Mattila et al. (2012) estimate SNe CC rates of almost  $2(10^{-4}) \text{ yr}^{-1} \text{ Mpc}^{-3} h_{70}^3$ , the works of Cappellaro et al. (1999) and Li et al. (2011) give SNe CC rates of the order of  $0.6(10^{-4}) \text{ yr}^{-1} \text{ Mpc}^{-3} h_{70}^3$ . The model outputs are consistent with the higher values of SNe CC rates at  $z = 0$ .

The SNe Ia rates shown in Fig. 8 for different values of  $\alpha_{\text{TH}}$  are compared with the one emerging from Salpeter IMF. We can see that for a value of  $\alpha_{\text{TH}}$  equal to the slope of Salpeter IMF, the TH-IGIMF gives larger values of SNe Ia rates since the differences between both IMFs for stellar masses smaller than  $1.3 M_{\odot}$  lead to different normalization values. Once both SAGS and SAGTH5B2 have been calibrated, the SNe Ia rates are similar in both models, as can be seen from the comparison of dashes and solid lines in Fig. 9.

The CC SNe in the model have delay times between 2 and

30 Myr (top panel of Fig. 8), sufficiently short for the forming stars in a burst to lock most of the  $\alpha$ -elements produced during the explosions, since the actual duration of bursts have longer timescales, of the order of tens of Myr (see Fig. 6). On the other hand, the delay times of SNe Ia are in the range comprised between tens of Myr and some Gyr, with the bulk of SNe Ia having delay times between 20 Myr – 2 Gyr with a peak at approximately 100 Myr.

This time-scale is of the order of the maximum value of the starbursts duration, therefore many starbursts will not form stars highly enriched with the main SNe Ia product, that is, iron. However, since the starbursts do not consume the cold gas bulge instantaneously, it is frequent that several bursts coexist in a same galaxy and a late triggered one might form stars rich in iron from gas polluted by a previous generation of stars formed in the bulge. Hence, the final  $[\alpha/\text{Fe}]$  abundance ratio of an elliptical galaxy is the result of the combination of the duration of starbursts, SNe delay times and time-scale of galaxy formation. The latter is analysed in detail for both SAGS and SAGTH5B2 models in Section 5.

### 4.3 Further tests: mass-to-light ratios and luminosity functions

Matteucci (1994) suggested that the variable IMF hypothesis to explain the  $[\alpha/\text{Fe}]$ -mass relation in elliptical galaxies should be tested on integrated luminosities and mass-to-light ratios (M/L).

In a series of papers, the ATLAS3D collaboration study the properties of a sample of 260 early-type galaxies (see Cappellari et al. 2011). In paper XV (Cappellari et al. 2013) and XX (Cappellari et al. 2013) they concentrate on the mass plane ( $M$ ,  $\sigma_e$ ,  $R_e$ ), its projections, and the distribution of galactic properties among them. They derive total (baryonic plus dark matter) dynamical masses and mass-to-light ratios ( $M_{\text{JAM}}$ ,  $M/L_{\text{JAM}}$ ) within a sphere of one effective radius of the early type galaxies in their sample. They point out that this quantity resembles and is directly comparable to the total stellar mass used in previous studies, given that the calculated fraction of DM inside that radius is usually low, 13% on average. They choose the Sloan  $r$ -band to measure luminosities. It is worth noting that these quantities are unaffected by assumptions on the IMF in galaxies because they are derived using dynamical considerations and their calculations do not involve stellar population synthesis models. In Fig. 10 we compare the mass-to-light ratio as a function of the stellar mass of elliptical galaxies resulting from our model with Salpeter IMF (top panel) and SAGTH5B2 (bottom panel), with the data extracted from Table 1 of Cappellari et al. (2013). For this purpose, we consider the stellar mass of model galaxies divided by the total luminosity in the  $r$ -band. The error at  $1\sigma$  of the estimations of M/L ratios from Cappellari et al. (2013) is 0.027 dex. We can see that in the case of our best choice of the TH-IGIMF parameters, that is,  $\beta = 2$  and  $M_{\text{ecl}}^{\text{min}} = 5 M_{\odot}$ , the zero point of the relation is better reproduced than in model SAGS, with a good agreement with the observed M/L ratios in a broad range of stellar masses. The departure from observations occurs for masses smaller than  $2 \times 10^{10} M_{\odot}$ , for which the slopes of the IMF are steeper than the one of Salpeter IMF (see Fig. 5). The shape of the M/L ratios is similar for both SAGS and SAGTH5B2 models, with lower values for the latter case and a higher dispersion towards lower values, as a result of the calibration process that regulates in a different way the star formation and feedback. That is, it seems that the IMF helps to recover the correct values of the M/L ratios for massive galaxies, but it cannot solve the problem of the excess at lower masses with respect to observations,

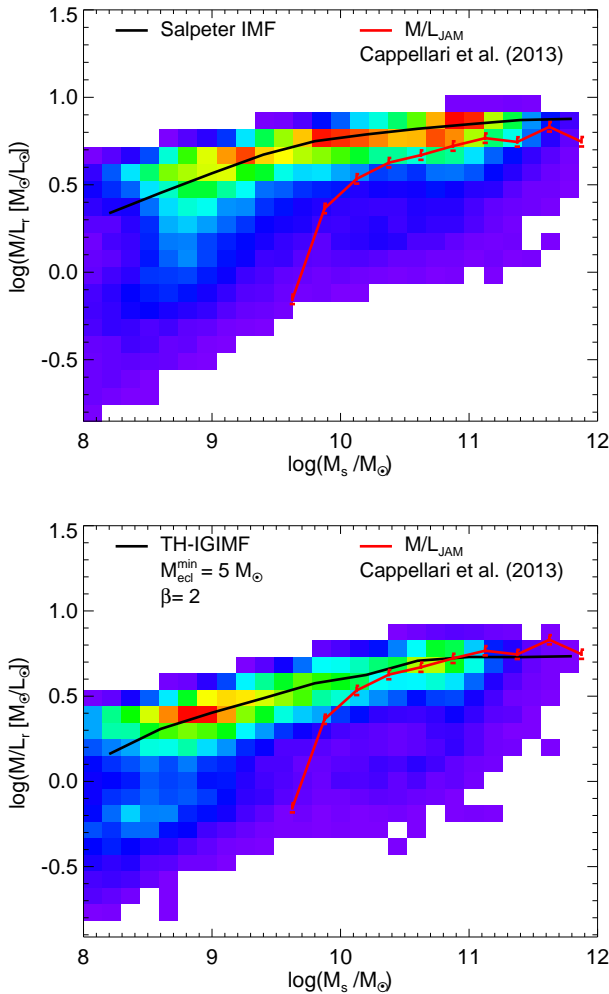


**Figure 10.** Mass-to-light Ratios as a function of the stellar mass of elliptical galaxies. Results from models SAGS and SAGTH5B2 are shown in the top and bottom panels, respectively, compared with observational determinations of (Cappellari et al. 2013).

which is present for any IMF. This result supports the hypothesis of a TH-IGIMF in elliptical galaxies.

We perform a further test to the population of galaxies. We compare the results from models SAGS and SAGTH5B2 with the observed  $r$ -band LF of Blanton et al. (2005), used as a constraint to calibrate the model. The  $r$ -band LFs resulting from both models are shown in Fig. 11. As can be seen, there are not major differences between them and the agreement with the observed LF (Blanton et al. 2005) is quite good. A slight excess of luminous galaxies is present in both models, being more notorious in the model SAGS. The suppression of SF in the most massive galaxies cannot be achieved with the current modelling of AGN feedback. Instead, a better agreement with observations could be obtained if starbursts during galaxy mergers are triggered only when the remnant galaxy becomes unstable, as proposed by Padilla et al. (2014). The luminosity function together with the mass-to-light ratios represent a good test to the implementation of a variable IMF, given that different stellar populations are characterized by distinct signatures of light that must be constrained together with the  $[\alpha/\text{Fe}]$ -mass relation in order to obtain consistent results in the properties of galaxies when modifying an important distribution function like the IMF of stars.

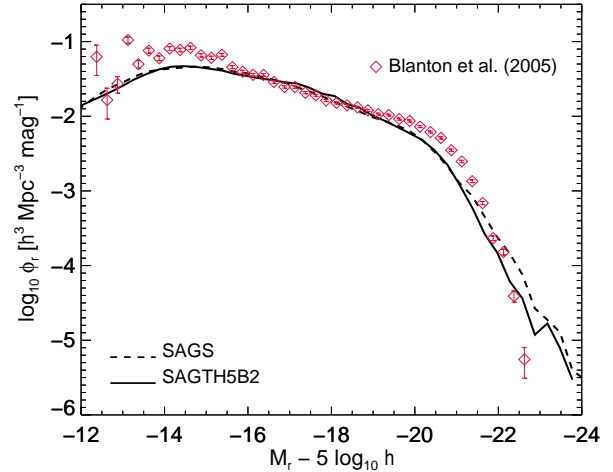


**Figure 11.** Luminosity function in the  $r$ -band of the population of galaxies generated by models SAGS (dashed line) and SAGTH5B2 (solid line) compared with the observed determinations by Blanton et al. (2005) (open symbols with error bars).

## 5 $[\alpha/\text{Fe}]$ -MASS RELATION: INFLUENCE OF FORMATION TIME-SCALES

In this work, we have demonstrated that a TH-IGIMF is needed to reproduce the trend of  $[\alpha/\text{Fe}]$  abundance ratios with stellar mass shown by elliptical galaxies. However, one aspect also considered to explain the built-up of this relation is the time-scale of galaxy formation. This argument claims that more massive galaxies are formed in a shorter time-scale than less massive ones (e.g. Thomas et al. 2005; Recchi et al. 2009). In this sense, this relation is usually considered as another consequence of the downsizing. Observational evidence indicates that elliptical galaxies assemble most of their mass at high redshift. A common technique used nowadays is the stellar archaeology (Thomas et al. 2005; Neistein et al. 2006). In this line of work, spectral indices are measured and used to compute parameters of stellar populations of observed galaxies with population synthesis models. One common result of applying this method is that stellar populations in massive galaxies are older than in their less massive counterparts, disregarding the galaxy morphology (Panter et al. 2007). Moreover, elliptical galaxies present the oldest stellar populations, given that they show little or none star formation activity, although T10 find that approximately 10 per cent of their sample of ellipticals are actively forming stars and define a peak at young ages in the age distribution. Neistein et al. (2006) find that this aspect of the downsizing behaviour of galaxies can be explained naturally in the frame of hierarchical clustering in terms of the progenitors of the main haloes, defining a minimum mass of progenitors that are capable of forming stars. However, other aspects also considered as downsizing, like the shift with time in the characteristic mass of star forming galaxies (Cowie & Barger 2008), or the chemo-archaeological downsizing (Fontanot et al. 2009) can not be explained with this line of reasoning.

Here, we are focusing on the chemo-archaeological downsizing. The aim of this section is to analyse the formation time-scales of our sample of model galaxies in order to determine whether they are partially responsible for leading to a positive slope in the  $[\alpha/\text{Fe}]$ -stellar mass relation or not.



For each galaxy selected according to its stellar mass at  $z = 0$ , we define the formation time-scale,  $\Delta T_{50}$ , as the period of time elapsed since the redshift at which the first star formation event occurs and the formation redshift,  $z_{\text{form}(50)}$ . The latter is defined as the redshift at which the galaxy acquires 50 per cent of its total stellar mass formed *in-situ*, where the term *in-situ* refers to the stellar mass formed in a galaxy by quiescent SF or in starbursts, without taking into account the stars of accreted satellites. This definition ensures that the analysed galaxies and their stellar populations are formed from enriched gas belonging to their main progenitors, making easier the interpretation of the influence of star formation time-scales and ejection of SNe products on the  $[\alpha/\text{Fe}]$ -stellar mass relation. Note that the total stellar mass formed *in-situ* considered for the present analysis is tracked in a separate variable within the code, and does not take into account the effect of mass loss due to the recycling process.

Fig. 12 shows the formation time-scale,  $\Delta T_{50}$ , as a function of the formation redshift,  $z_{\text{form}(50)}$ , for our whole sample of early-type galaxies obtained from models with two different IMFs. We consider the models SAGTH5B2 (top panel) and SAGS (bottom panel) which involve a TH-IGIMF with parameters  $M_{\text{ecl}}^{\text{min}} = 5 M_{\odot}$  and  $\beta = 2$  and the Salpeter IMF, respectively. The former is our selected best case of TH-IGIMF, as discussed in the previous section. We can see that, regardless of the IMF considered, there is a clear trend in which  $\Delta T_{50}$  decreases as  $z_{\text{form}(50)}$  increases, as depicted by the colour-density plot. This indicates that galaxies that form at higher redshift complete the formation process in shorter time-scales, consistent with Lagos, Padilla & Cora (2009). More specifically, galaxies that have formed at  $z_{\text{form}(50)} \approx 2$  or before took less than 2 Gyr to achieve 50 per cent of their stellar mass formed *in-situ*.

At lower redshifts, the dispersion in the formation time-scales becomes larger. The histograms on the top and on the right of the central panel, in both the top and bottom plots, are the frequency distributions of the formation redshift and the formation time-scale, respectively. We see that the bulk of early type galaxies form between  $z_{\text{form}(50)} \approx 1$  and 0 and in time-scales within a range  $1 \text{ Gyr} \lesssim \Delta T_{50} \lesssim 4 \text{ Gyr}$ . If we consider the global population of galaxies formed at different redshifts, we find that most of the galaxies have formation time-scales less than 2 Gyr, as it is evident from the histograms on the right. The mean and median values of the distributions of  $\Delta T_{50}$  (dotted and dashed lines in the figure, respectively) are 2.32 Gyr and 1.94 Gyr for model SAGTH5B2, and 2.51 Gyr and 2.02 Gyr for model SAGS, respectively. For the distributions of  $z_{\text{form}(50)}$ , we have mean and median values of 1.2 and 0.97 for SAGTH5B2, and 1.18 and 0.97 for SAGS, respectively.

The distributions of  $z_{\text{form}(50)}$  for galaxies of different mass are shown in Fig. 13 for models SAGTH5B2 and SAGS (top and bottom panels, respectively). In agreement with a previous study by Lagos et al. (2009), both models present similar shapes of their  $z_{\text{form}(50)}$  distributions for different mass ranges. We see that the least massive galaxies ( $M_{\star} < 10^9 M_{\odot}$ ) achieve the 50 per cent of their stellar mass formed *in-situ* at lower redshifts than more massive galaxies, with the bulk of them forming between  $z \approx 0$  and  $z \approx 0.5$ . The downsizing trend is less pronounced for galaxies more massive than  $\approx 10^9 M_{\odot}$ . The mean and median values of the distributions (denoted by dotted and dashed lines, respectively) are pretty similar for galaxies with masses within the ranges  $10^9 - 10^{10} M_{\odot}$  and  $10^{10} - 10^{11} M_{\odot}$ , and  $10^{11} M_{\odot}$ , with values comprised within the interval  $1 \lesssim z_{\text{form}(50)} \lesssim 1.5$ . However, the peak of the corresponding distributions shifts from the interval  $0 \lesssim z_{\text{form}(50)} \lesssim 0.5$  to  $0.5 \lesssim z_{\text{form}(50)} \lesssim 1$ , making evident a mild

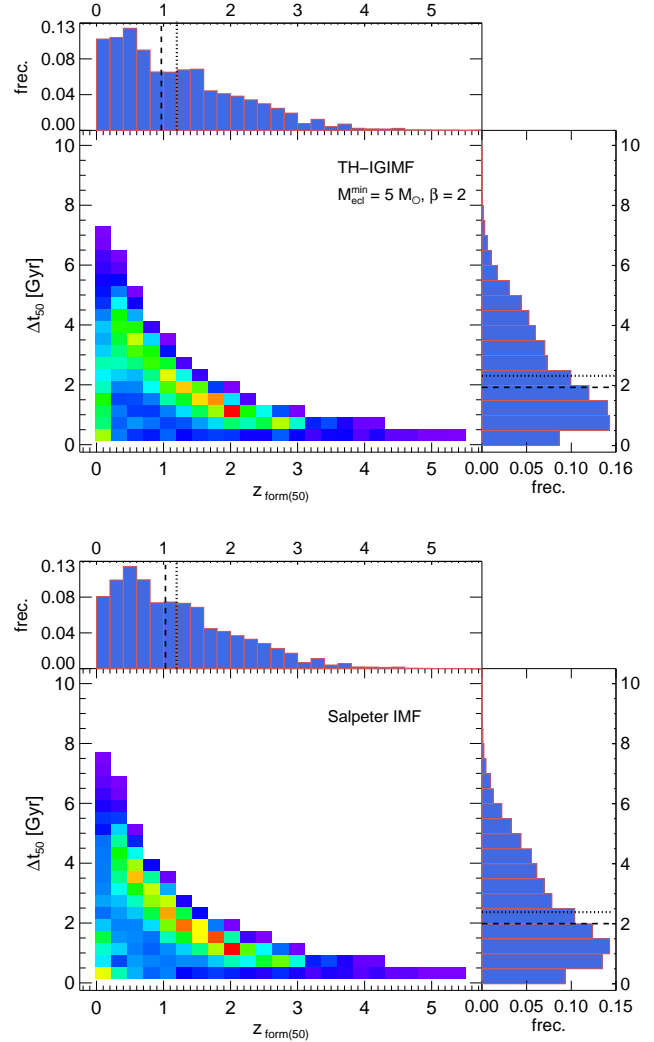


**Figure 12.** Formation time-scales,  $\Delta T_{50}$ , of elliptical galaxies from the models versus their formation redshifts,  $z_{\text{form}(50)}$  (see plain text for the definition) for galaxies from model SAGTH5B2 (top panel) and SAGS (bottom panel). The histograms on the right of central panels are the frequency distributions of the formation time-scales of the galaxy population, and those on the top correspond to the formation redshifts. Dotted and dashed lines represent the mean and median values of the distributions, respectively.

downsizing trend. The shift of the peak of the distributions is more evident in the model SAGS (lower panel). This is in qualitative agreement with Lagos et al. (2009) and De Lucia et al. (2006). In the latter work, it is shown that massive galaxies form their stars earlier than less massive systems but that they assemble their stars later. They define the formation redshift as the redshift when 50 per cent of the stars that make up the galaxy at redshift  $z = 0$  are already formed, and the assembly time as the redshift when 50 per cent of the final stellar mass is already contained in a single object. In our definition of formation time, we are not considering the contribution of the stellar mass formed in accreted satellite galaxies. We have tested the impact of this accreted mass on the histograms shown in Fig. 13, and we do not find any significant change, neither for SAGTH5B2 nor for SAGS. This is expected taking into account that the mass contributed by satellites is a small fraction of the total final mass of the galaxy, being of the order of  $\approx 10$  per cent for the

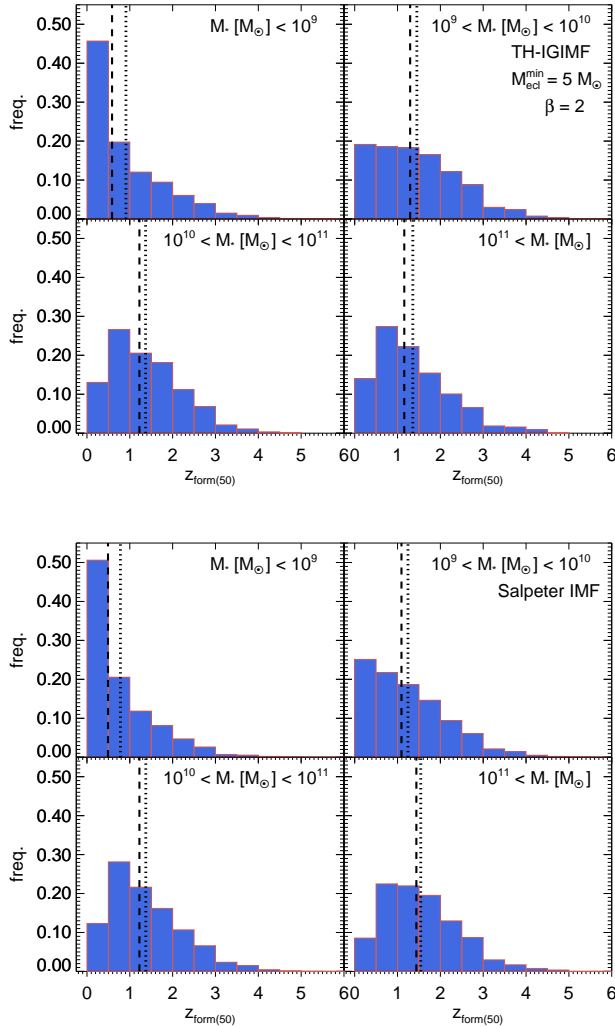


**Figure 13.** Distribution of formation redshifts,  $z_{\text{form}(50)}$ , for galaxies of different stellar mass, as indicated in the key for models SAGTH5B2 (top panel) and SAGS (bottom panel). Dotted and dashed lines represent the mean and median values of the distributions, respectively.

vast majority of galaxies, in agreement with the analysis done by Jiménez et al. (2011).

We now focus on the distributions of  $\Delta T_{50}$  considering galaxies in different mass ranges. This is shown in Fig. 14 for both SAGTH5B2 and SAGS models (top and bottom panels, respectively). As in the distributions for the whole galaxy population (Fig. 12), the mean and median values (dotted and dashed lines, respectively) are very close to each other. The main aspect to emphasize is that they are very similar to the values corresponding to the complete sample of galaxies ( $\approx 2 - 2.5$  Gyr) and do not present a great dependence with stellar mass; only most massive galaxies ( $M_* > 10^{11}$ ) in model SAGTH5B2 have slightly larger mean and median values of  $\Delta T_{50}$ . This situation is pretty similar for both models, indicating that the time-scales of galaxy formation are not strongly affected by the choice of the IMF. To put in context these galactic formation time-scales, we make a comparison with the time-scales needed to reproduce the right  $[\alpha/\text{Fe}]$ -mass relation in the model of Pipino & Matteucci (2004). Their models reproduce right slopes of  $[\alpha/\text{Fe}]$  as a function of galactic mass assuming early infall of

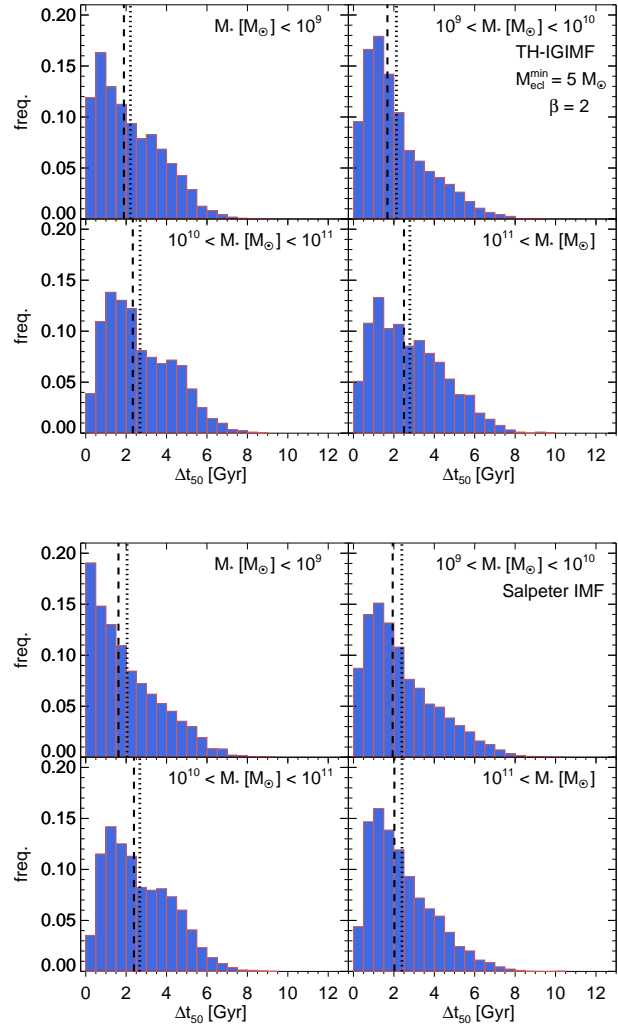


**Figure 14.** Distribution of formation time-scale,  $\Delta T_{50}$ , for galaxies of different stellar mass, as indicated in the key for models SAGTH5B2 (top panel) and SAGS (bottom panel). Dotted and dashed lines represent the mean and median of the distributions, respectively.

gas with time scales of the order of 0.4 Gyr and galactic winds that last no longer than 0.7 Gyr, within the paradigm of monolithic collapse, which explains the differences with our time-scales of galaxy formation.

The mild dependence of the formation time-scales with stellar mass that emerges from our models, with a Salpeter IMF or a TH-IGIMF, shows a trend opposite to the one found by De Lucia et al. (2006). Based on the analysis of the star formation histories of galaxies obtained from a semi-analytic model, they show that massive elliptical galaxies have shorter star formation time-scales than less massive ones, in qualitative agreement with the downsizing scenario (Cowie et al. 1996) and with the stellar mass time-scale dependence required by Thomas et al. (2005) in order to explain the observed  $[\alpha/\text{Fe}]$ -stellar mass relation. The different trends obtained from our models and those of De Lucia et al. (2006) are not explained by the fact that we are not considering the star formation taking place in accreted satellites in our definition of formation time-scale; as in the distributions of formation redshift, we evaluate the influence of the stellar mass in accreted satellites finding no

significant change. Note, however, that the extensions of the time interval in which the star formation takes place present small differences between galaxies in different mass ranges, both in our sample of model galaxies and in those of De Lucia et al. (2006).

This mild downsizing trend that emerges from our model, as shown by the  $z_{\text{form}(50)}$  distributions and the almost null differences of  $\Delta T_{50}$  between galaxies of different masses minimize the relevance of the most accepted explanation to interpret the larger  $[\alpha/\text{Fe}]$  abundance ratios in more massive galaxies, which is generally attributed to their relatively short formation time-scales as inferred from the analysis of observational data (e.g. Thomas et al. 2005). If this difference in the formation timescales were present in real galaxies, it would contribute to the development of a positive slope of the relation as shown in other galaxy formation models (e.g. Pipino & Matteucci 2004). However, this explanation of the chemo-archaeological downsizing could be discarded if we take into account the lack of strong evidence of downsizing in terms of differential evolution of the stellar mass assembly or for differential evolution of the SFR density for galaxies of different mass as emerge from the analysis of several observational data set (Fontanot et al. 2009; Sobral et al. 2014). Our models support the possibility that massive galaxies reach higher  $[\alpha/\text{Fe}]$  abundance ratios because they are characterized by top-heavier IMFs. Our study reinforces this idea because of the similarity of the  $z_{\text{form}(50)}$  and  $\Delta T_{50}$  distributions and of the relation between them for models with a Salpeter IMF and a TH-IGIMF, indicating that the time-scales of galaxy formation do not play a decisive role in determining the slope of the  $[\alpha/\text{Fe}]$ -stellar mass relations followed by galaxies generated by these two models. The most relevant result of our work is that a TH-IGIMF is necessary to reproduce the observed trend. We have to bear in mind that, although our model present a mild downsizing in terms of the characteristic redshift of galaxy formation and time-scales of star formation, the latter is the quantity that matters in the interpretation of the  $[\alpha/\text{Fe}]$ -stellar mass relation. However, the main observational evidence of downsizing in terms of these time-scales is inferred from the relation itself.

From this important result, we consider galaxies from model SAGTH5B2 and analyse the link between the distribution of  $[\alpha/\text{Fe}]$  abundance ratios and the formation time-scale  $\Delta T_{50}$  in order to understand the origin of the main features of the  $[\alpha/\text{Fe}]$ -stellar mass relations of galaxies with a TH-IGIMF characterized by  $M_{\text{ecl}}^{\text{min}} = 5 M_{\odot}$  and a slope the mass function of embedded clusters  $\beta = 2$ . This is shown in Fig. 15, where the different panels correspond to galaxies within different mass ranges. In all cases, we can see that larger values of  $[\alpha/\text{Fe}]$  abundance ratios are achieved for shorter formation time-scales. The important aspect to emphasize is that the time-scales argument allows to explain the dispersion of  $[\alpha/\text{Fe}]$  values for galaxies of a given mass, but is not the reason of the development of an  $[\alpha/\text{Fe}]$ -stellar mass relation with a positive slope. This dependence between the  $[\alpha/\text{Fe}]$  abundance ratios and the stellar mass is only possible by considering a SFR dependent IMF like the TH-IGIMF tested here.

Linking the result shown in Fig. 15, which indicates that galaxies with shorter formation time-scales have larger values of  $[\alpha/\text{Fe}]$  abundance ratios, with that appreciated from Fig. 12, where it is clear that older galaxies (those with higher  $z_{\text{form}(50)}$ ) are formed in shorter time-scales, we conclude that older galaxies achieve larger values of  $[\alpha/\text{Fe}]$  abundance ratios. This is consistent with the observational data analysed by Sánchez-Blázquez et al. (2006), who find that the models that better reproduce the observed slopes are those in which the  $\alpha$ -elements vary more than the Fe-peak elements along the sequence of velocity dispersion; moreover,

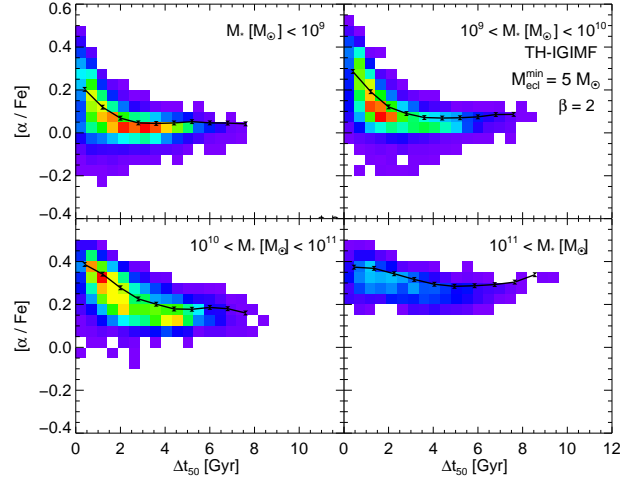


**Figure 15.** Distributions of  $[\alpha/\text{Fe}]$  abundance ratios as a function of the formation time-scale,  $\Delta T_{50}$ , for galaxies within different mass ranges, as indicated in the key, for model SAGTH5B2, characterized by  $M_{\text{ecl}}^{\text{min}} = 5 M_{\odot}$ . The solid line in each panel connects the mean values of  $[\alpha/\text{Fe}]$  abundance ratios for different bins of  $\Delta T_{50}$ .

older galaxies at a given velocity dispersion show higher  $[\alpha/\text{Fe}]$  abundance ratios. These results also support previous findings by Trager et al. (2000), who show that younger ellipticals have higher  $[\text{Fe}/\text{H}]$  abundances than older ones.

## 6 DISCUSSION

The trend of  $[\alpha/\text{Fe}]$  with stellar mass in early type galaxies has been studied in the past, both observationally and theoretically. Regardless of the observational methods, there is agreement that the relative abundances of light elements (produced almost exclusively by SNe CC) with respect to iron (produced mainly by SNe Ia) increase monotonically with galaxy central velocity dispersion (hence, galaxy mass). On the theoretical side, a considerable deal of work has been devoted to study this aspect of chemical evolution within the framework of the cosmological model  $\Lambda$ -CDM, mainly because it has been pointed out as a problem of the model, showing tension between the expected hierarchical bottom-up growth of structure and the downsizing behaviour of galaxies. Two main hypotheses have been proposed to explain the observed trend, the time-scale of galaxy formation and the variable IMF. In the time-scale argument, the stellar populations in galaxies with higher stellar masses are assumed to form in shorter time-scales, avoiding the enrichment of their ISM by SNe Ia that are characterized by long explosion delay-times. In the case of the variable IMF hypothesis, the variable high-mass to low-mass stars ratio in the initial distribution of stars in different galaxies is assumed to play a crucial role in the building-up of the observed abundance pattern in early-type galaxies, given that this ratio determines the SNe CC to SNe Ia ratio.

In the last years, there have been several studies of massive early type galaxies suggesting that their stellar populations might have been formed with IMFs different from those found in the solar neighbourhood. There are indications that the light of stars in massive early type galaxies is consistent with populations formed with a bottom-heavy IMF, as given by the analysis of their spectral features (van Dokkum & Conroy 2010, 2012;

Ferreras et al. 2013; La Barbera et al. 2013; Conroy et al. 2013); in other works, the mass-to-light ratio of massive early type galaxies is constrained by using dynamical tools (Cappellari et al. 2012; Dutton et al. 2012; Tortora et al. 2013) or strong gravitational lensing (Auger et al. 2010; Treu et al. 2010). However, these methods present a degeneracy in the sense that a higher ratio of less massive stars implies either a bottom heavy IMF or a top heavy IMF, since massive stars end their lives in short time-scales and contribute to the total emitted light only during star formation events and shortly after. Weidner et al. (2013) study the problem with a toy model that proposes a top heavy IMF at high redshift during early starbursts conditions and a bottom heavy IMF in the subsequent evolution. In their model, the high star formation regime drives the fragmentation of the ISM favouring the formation of low-mass stars. One important aspect they remark is that the bottom heavy IMF proposed by several works, like Ferreras et al. (2013), can underestimate severely the amount of metals present in massive elliptical galaxies, given that most metals are ejected to the ISM by stars with masses above  $1 M_{\odot}$ .

In general, when the argument of a variable IMF is considered to explain the  $[\alpha/\text{Fe}]$ -stellar mass relation, the proposed IMF is treated as a free parameter (Arrigoni et al. 2010), or is varied with exploratory aims (Thomas 1999; Nagashima et al. 2005; Calura & Menci 2009), following no particular theory and leaving unexplored a vast region of the corresponding parameter space. In this work, we test the well defined theory regarding the integrated initial mass function of stars in galaxies with top heavy IMFs in star clusters during starbursts (see Subsection 2.3 for a brief description and references for the original papers). We have shown that the  $[\alpha/\text{Fe}]$  abundance ratio is well reproduced by assuming a SFR dependent TH-IGIMF; our results support a value of  $5 M_{\odot}$  for the minimum embedded star cluster mass and of  $\beta = 2$  for the slope of the embedded cluster mass function, which are free parameters in this theory. Recchi et al. (2009, R09 hereafter) have already considered the IGIMF theory to evaluate the impact in the build-up of the  $[\alpha/\text{Fe}]$  -  $\sigma$  relation and explore different values for the slope of the embedded cluster mass function ( $\beta$  1, 2 and 2.35). They make use of a previous version of the IGIMF, where the effect of high levels of star formation in galaxies was not considered. When these high levels of SF are attained, the IMF within clusters can become top heavy due to effects of crowding. In such conditions, the SFR dependence changes with the consequent reduction in the values of the slopes of the IGIMF in the TH-IGIMF version. There are important differences between the models used in R09 and those used in this paper. We make use of a semi-analytical model with merger trees that considers the evolution of elliptical galaxies in the framework of a  $\Lambda$ -CDM Universe. The analytical model used in R09 considers the evolution of elliptical galaxies from the point of view of the monolithic collapse. Another fundamental aspect is the treatment of the stellar and AGN feedback. Our model takes into account the feedback produced by stars consistently with the choice of the TH-IGIMF slope. This means that lower values of the slopes of the TH-IGIMF lead to higher numbers of SNe CC that reheat cold gas, regulating the formation of new generations of stars and placing strong constraints on the free parameters of the TH-IGIMF theory. For example, for  $M_{\text{ecl}}^{\text{min}} = 100 M_{\odot}$  or even for the slope of the embedded star cluster  $\beta = 2.1$ , we find it difficult to calibrate the model given the high levels of SNe feedback. Feedback of AGNs in galaxies, which is not considered in the models of R09, is also an important aspect because it prevents massive galaxies to continue forming stars at low redshifts. This contributes to

determine the mild downsizing trend seen in our model although a more strong effect would be expected.

An associated problem to the  $\alpha$ -element abundances in early-type galaxies is related to the calcium (Ca) abundances. It is commonly expected that all the light elements produced by  $\alpha$ -capture track each other as a result of their common origin. However, the Ca abundance with respect to iron does not follow the magnesium (Mg) or titanium (Ti) abundance relative to iron as a function of central velocity dispersion (or galaxy mass) in early type galaxies. While the spectral indices sensitive to Mg or Ti show an increase of their abundances with increasing mass, some indices sensitive to Ca show a decrease of the abundance of this element with mass (Saglia et al. 2002; Cenarro et al. 2003, 2004). Recently Worthey et al. (2013) confirm this puzzling trend with new observations and evaluate different hypothesis to explain it. They find that a steepening of the IMF at low-mass stars is ruled out by constraints on galaxy colours. Interestingly, an IMF favouring the formation of massive stars is in agreement with their results, provided that the used stellar yield of Ca depends on the progenitor mass of SNe CC. Yields from Woosley & Weaver (1995) show a decrease of Ca with respect to iron with increasing mass of the progenitor star. However, Nomoto et al. (2006) and Kobayashi et al. (2006) show no dependence of the Ca yield with progenitor mass. If this trend of the SNe CC stellar yields of Ca is real, a top heavy IMF, as the one tested in this paper, would be needed to explain the calcium correlation with mass of early type galaxies, since the formation of massive stars would be favoured during the formation of more massive galaxies.

Recent work by Conroy et al. (2013) show more interesting trends between other individual elements. They study the abundance patterns of barium (Ba) and strontium (Sr) and find that the relative abundance ratio  $[\text{Ba}/\text{Mg}]$  show a decrease with respect to  $[\text{Mg}/\text{Fe}]$  and, although not shown in their work, they claim a strong correlation between  $[\text{Mg}/\text{Ba}]$  and velocity dispersion in a sample of early-type galaxies drawn from the SDSS. The importance of this finding lies in the fact that Ba is an element that is produced by the s-process in low and intermediate mass stars during the phase of asymptotic giant branch (AGB) in their evolution. Thus, the abundance ratio  $[\text{Mg}/\text{Ba}]$  can be used as a probe of short formation time-scales as well as an indicator of high mass to low mass stars ratio, just like the  $[\text{Mg}/\text{Fe}]$  ratio. But this is more than an alternative measure because it permits to set aside the influence of SNe Ia. Consequently, if real, this new abundance pattern would allow to rule out some explanations for the  $[\alpha/\text{Fe}]$ -stellar mass relation in early-type galaxies involving different delay-times distributions for SNIa (e.g. Yates et al. 2013). In a future paper, we will analyse the behaviour of these individual trends in our semi-analytic model in order to shed light on these issues.

We point out here a drawback in our chemical implementation, also present in other semi-analytic models (e.g. Yates et al. 2013). We consider, for simplicity, that yields from winds of low- and intermediate-mass stars, estimated as the integral of the metal ejection taking place during their entire evolutions, are deposited in the ISM at the end of their lives. Low and intermediate mass stars (LIMS) have long lives, and most of them still exist at the time of the final simulation output. Therefore, we consider that the gradual ejection of metals from LIMS could affect our results. We will also tackle this problem in a future work, analysing also the dependence of the stellar yields with the metallicity of the stars.

## 7 CONCLUSIONS

We use a model of galaxy formation that combines a dissipation-less cosmological  $N$ -body simulation with the semi-analytic model of galaxy formation and evolution SAG (Cora 2006; Lagos et al. 2008; Tecce et al. 2010) to study the physical aspects behind the build-up of the  $[\alpha/\text{Fe}]$ -stellar mass relation of elliptical galaxies, known as chemo-archaeological downsizing (Fontanot et al. 2009). A version of the semi-analytic model SAG that involves the Salpeter IMF (model SAGS) is not able to reproduce the right slope of the  $[\alpha/\text{Fe}]$ -stellar mass relation once the modelling of several aspects of SAG have been improved (like the starburst time-scales).

Earlier attempts to model the abundance of  $[\alpha/\text{Fe}]$  have failed to reproduce the observed relation with stellar mass, unless when invoking ad hoc hypotheses, like a change in the slope of the global IMF (Arrigoni et al. 2010), an arbitrary SFR-dependent IMF (Calura & Menci 2009), starbursts in progenitor galaxies triggered by close encounters (Calura & Menci 2011) or empirically adopted SNIa delay times (Yates et al. 2013). Motivated by our finding that a universal IMF does not naturally allow to reproduce the right slope in the observed trend between the  $[\alpha/\text{Fe}]$  abundance ratio and the stellar mass of elliptical galaxies, we explore the impact of a variable IMF on their  $[\alpha/\text{Fe}]$ -stellar mass relation. We have achieved  $[\alpha/\text{Fe}]$  abundance ratios for different stellar mass consistent with those found in observations, by implementing in our semi-analytic model a SFR dependent IMF that results from a physically motivated theory (TH-IGIMF, WKP11). The consistency of this implementation and the fact that many other observational galaxy properties and relations are simultaneously reproduced, make our conclusions more robust. We find that the use of a TH-IGIMF to represent the galaxy-wide IMF is necessary for a proper treatment of the chemical enrichment of galaxies. We summarize the main results of our work:

- A galaxy formation model with a TH-IGIMF can recover the positive slope of the observed  $[\alpha/\text{Fe}]$ -stellar mass relation (Fig. 4). This is the case for the two test values considered for the minimum embedded star cluster mass ( $M_{\text{ecl}}^{\text{min}} = 5$  and  $100, M_{\odot}$ ), and the two values considered for the slope of the embedded star cluster mass function  $\beta = 2$  and  $2.1$  which are free parameters involved in the TH-IGIMF theory. However, the agreement with the observational trend is particularly good for  $M_{\text{ecl}}^{\text{min}} = 5 M_{\odot}$  and  $\beta = 2$ . Thus, our results favour a small value for the minimum embedded star cluster mass and the standard value for the slope of the embedded star cluster mass function.
- Regardless of the value of  $M_{\text{ecl}}^{\text{min}}$  and  $\beta$ , the mean slope of a TH-IGIMF ( $\langle\alpha_{\text{TH}}\rangle$ ) becomes progressively lower for more massive galaxies (Fig. 5). Since this slope is SFR-dependent, this behaviour is a manifestation of the fact that more massive galaxies have higher SFR. The relative difference of the IMF slope for galaxies with different masses is key to reproduce the observed  $[\alpha/\text{Fe}]$ -stellar mass relation. This is demonstrated by our best model, characterized by  $M_{\text{ecl}}^{\text{min}} = 5 M_{\odot}$  and  $\beta = 2$ ; in this case, the TH-IGIMF is steeper than the Salpeter IMF for half of the mass ranges, showing that a top heavy IMF in all galaxies is not a necessary condition in the build-up of the  $[\alpha/\text{Fe}]$ -stellar mass relation as generally believed. Our results indicate that galaxies with masses smaller than  $\sim 3 \times 10^{10} M_{\odot}$  should have IMF steeper than Salpeter IMF, while galaxies with higher masses should take top-heavier IMF than Salpeter IMF in order to achieve the right chemical abundances.

- A mild downsizing trend is evident for galaxies generated by models with different IMF. The distributions of the formation redshift ( $z_{\text{form}(50)}$ ) and formation time-scale ( $\Delta T_{50}$ ) of elliptical galax-

ies generated from models SAGTH5B2 and SAGS, characterized by a TH-IGIMF with  $M_{\text{ecl}}^{\text{min}} = 5 M_{\odot}$  and  $\beta = 2$  and the Salpeter IMF, respectively, have similar features and dependence with stellar mass (Figs. 13 and 14) supporting the fact that the choice of the IMF has negligible effect on the time-scales of galaxy formation. In both cases, the least massive galaxies ( $M_{*} < 10^9 M_{\odot}$ ) achieve the 50 per cent of their stellar mass formed in-situ at lower redshifts than more massive ones, with the bulk of them forming between  $z \approx 0$  and  $z \approx 0.5$ ; the peak of the distributions for galaxies more massive than  $\approx 10^9 M_{\odot}$  shifts from the interval  $0 \lesssim z_{\text{form}(50)} \lesssim 0.5$  to  $0.5 \lesssim z_{\text{form}(50)} \lesssim 1$ . The distributions of  $\Delta T_{50}$  are very similar for galaxies of different mass, displaying values corresponding to the complete sample of galaxies ( $\approx 2 - 2.5$  Gyr). This mild downsizing trend present in models either with a universal or variable IMF indicates that the time-scale for galaxy formation does not play a decisive role in determining the slope of the  $[\alpha/\text{Fe}]$ -stellar mass relation, which does show important changes in our results when changing to the TH-IGIMF. It should be born in mind, though, that the mild downsizing is a feature of semi-analytic models. If the time scale for star formation is allowed to vary more freely, then it also helps to produce a dependence of  $[\alpha/\text{Fe}]$  on stellar mass. However, in this case, other properties of the galaxy population in a cosmological context might not behave properly. Using a semi-analytic model, we are able to fit the  $[\alpha/\text{Fe}]$ -stellar mass relation at the same time as the  $z=0$  LF produces concordant results with observations. This requirement poses extra limitations in SAMs, which we show can still provide a reasonable  $[\alpha/\text{Fe}]$ -stellar mass relation. Our conclusion does not rule out the influence of downsizing on the development of this relation; it is just that this effect is not strongly manifested in galaxy formation models.

- Older galaxies (those with higher  $z_{\text{form}(50)}$ ) are formed in shorter time-scales; galaxies that have formed at  $z_{\text{form}(50)} \approx 2$  or before have  $\Delta T_{50} \lesssim 2$  Gyr (Fig. 12). On the other hand, galaxies with shorter formation time-scales have larger values of  $[\alpha/\text{Fe}]$  abundance ratios (Fig. 15). Hence, older galaxies achieve larger values of  $[\alpha/\text{Fe}]$  abundance ratios in agreement with observational data (Sánchez-Blázquez et al. 2006; Trager et al. 2000). This correlation is present for galaxies of different mass, thus explaining the dispersion of the  $[\alpha/\text{Fe}]$ -stellar mass relation at a given stellar mass.

- Mass-to-light ratios of massive elliptical galaxies have similar shapes in both models SAGTH5B2 and SAGS, showing an excess for low mass galaxies ( $\lesssim 2 \times 10^{10} M_{\odot}$ ) with respect to observations (Fig. 10). However, model SAGTH5B2 allows to achieve the correct values of M/L ratios for massive galaxies, leading to a better agreement with observational data. The bright end of the  $r$ -band LF also behaves better in model SAGTH5B2 (Fig. 11).

From the interpretation of observational data (e.g. Thomas et al. 2005), a generally accepted explanation for the build-up of the  $[\alpha/\text{Fe}]$ -stellar mass relation has been the relatively short formation time-scales of massive galaxies. Based on this time-scale argument, we would obtain larger values of  $[\alpha/\text{Fe}]$  for these galaxies since they have lower possibilities to form stars from cold gas contaminated by products of SNe Ia. The detailed analysis performed in this work had the purpose of determining if the galaxy formation time-scales are responsible for the positive slope in the  $[\alpha/\text{Fe}]$ -stellar mass relation. From this investigation, we can conclude that this time-scale argument only allows to explain the dispersion of  $[\alpha/\text{Fe}]$  values for galaxies of a given mass, but cannot account for the observed  $[\alpha/\text{Fe}]$ -stellar mass relation. Our results, based on a hierarchical galaxy formation model, show that the presence of a SFR-dependent TH-IGIMF is

a valid explanation for the relation between the  $[\alpha/\text{Fe}]$  abundance ratios and stellar mass. A variable IMF which slope depends on the SFR gives different relative numbers of SNe Ia and SNe CC progenitors for each star formation event, which is a key aspect in the build-up of the  $[\alpha/\text{Fe}]$ -stellar mass relation. Massive galaxies reach higher  $[\alpha/\text{Fe}]$  abundance ratios because they are characterized by top-heavier IMFs as a result of their higher SFR.

## ACKNOWLEDGMENTS

We thank the referee for his/her helpful comments that allowed to improve this paper. This work was partially supported by the Consejo Nacional de Investigaciones Científicas y Técnicas (CONICET, Argentina), Universidad Nacional de La Plata (UNLP, Argentina), Instituto de Astrofísica de La Plata (IALP, Argentina) and Secretaría de Ciencia y Tecnología de la Universidad Nacional de Córdoba (SeCyT-UNC, Argentina). AO gratefully acknowledges support from FONDECYT project 3120181. IDG acknowledges support from Comisión Nacional de Investigación Científica y Tecnológica (CONICYT, Chile) and Pontificia Universidad Católica de Chile (PUC) projects PFB-06 and ACT-86 for an academic stay at PUC. SAC acknowledges grants from CONICET (PIP-220), Argentina, Agencia Nacional de Promoción Científica y Tecnológica (PICT-2008-0627), Argentina, and Fondecyt, Chile. AMMA acknowledges support from CONICYT Doctoral Fellowship program. TET acknowledges funding from GEMINI-CONICYT Fund Project 32090021, Comité Mixto ESO-Chile and Basal-CATA (PFB-06/2007). GB acknowledges support from the National Autonomous University of México, through grant IB102212-RR182212. This project made use of the Geryon cluster at the Centro de Astro-Ingeniería UC for most of the calculations presented.

## REFERENCES

- Anders E., Grevesse N., 1989, *Geochimica Cosmochimica Acta*, 53, 197
- Arrigoni M., Trager S. C., Somerville R. S., Gibson B. K., 2010, *MNRAS*, 402, 173
- Athanassoula E., 2013, *Bars and secular evolution in disk galaxies: Theoretical input*. p. 305
- Auger M. W., Treu T., Gavazzi R., Bolton A. S., Koopmans L. V. E., Marshall P. J., 2010, *ApJL*, 721, L163
- Benson A. J., Borgani S., De Lucia G., Boylan-Kolchin M., Monaco P., 2012, *MNRAS*, 419, 3590
- Bernardi M., Nichol R. C., Sheth R. K., Miller C. J., Brinkmann J., 2006, *AJ*, 131, 1288
- Bertschinger E., 2001, *ApJS*, 137, 1
- Binney J., Tremaine S., 2008, *Galactic Dynamics: Second Edition*. Princeton University Press
- Blanton M. R., Lupton R. H., Schlegel D. J., Strauss M. A., Brinkmann J., Fukugita M., Loveday J., 2005, *ApJ*, 631, 208
- Botticella M. T., Smartt S. J., Kennicutt R. C., Cappellaro E., Sereno M., Lee J. C., 2012, *A&A*, 537, A132
- Bruzual G., 2007, in Vallenari A., Tantaló R., Portinari L., Moretti A., eds, *From Stars to Galaxies: Building the Pieces to Build Up the Universe Vol. 374 of Astronomical Society of the Pacific Conference Series, Stellar Populations: High Spectral Resolution Libraries. Improved TP-AGB Treatment*. p. 303
- Bruzual G., Charlot S., 2003, *MNRAS*, 344, 1000
- Calura F., Menci N., 2009, *MNRAS*, 400, 1347
- Calura F., Menci N., 2011, *MNRAS*, 413, L1
- Cappellari M., Bacon R., Bureau M., Damen M. C., Davies R. L., de Zeeuw P. T., Emsellem E., Falcón-Barroso J., Krajnović D., Kuntschner H., McDermid R. M., Peletier R. F., Sarzi M., van den Bosch R. C. E., van de Ven G., 2006, *MNRAS*, 366, 1126
- Cappellari M., Emsellem E., Krajnović D., McDermid R. M., et al. 2011, *MNRAS*, 413, 813
- Cappellari M., McDermid R. M., Alatalo K., Blitz L., Bois M., Bournaud F., Bureau M., Crocker A. F., et al. 2012, *Nature*, 484, 485
- Cappellari M., McDermid R. M., Alatalo K., Blitz L., et al. 2013, *MNRAS*, 432, 1862
- Cappellari M., Scott N., Alatalo K., Blitz L., et al. 2013, *MNRAS*, 432, 1709
- Cappellaro E., Evans R., Turatto M., 1999, *A&A*, 351, 459
- Cavaliere A., Vittorini V., 2000, *ApJ*, 543, 599
- Cenarro A. J., Gorgas J., Vazdekis A., Cardiel N., Peletier R. F., 2003, *MNRAS*, 339, L12
- Cenarro A. J., Sánchez-Blázquez P., Cardiel N., Gorgas J., 2004, *ApJL*, 614, L101
- Chabrier G., 2003, *pasp*, 115, 763
- Chiosi C., Bressan A., Portinari L., Tantaló R., 1998, *A&A*, 339, 355
- Colaboration S., 2006, *ApJS*, 162, 38
- Conroy C., Dutton A. A., Graves G. J., Mendel J. T., van Dokkum P. G., 2013, *ApJL*, 776, L26
- Conroy C., van Dokkum P. G., Graves G. J., 2013, *ApJL*, 763, L25
- Conselice C. J., 2006, *MNRAS*, 373, 1389
- Cora S. A., 2006, *MNRAS*, 368, 1540
- Cowie L. L., Barger A. J., 2008, *ApJ*, 686, 72
- Cowie L. L., Songaila A., Hu E. M., Cohen J. G., 1996, *AJ*, 112, 839
- Croton D. J., Springel V., White S. D. M., De Lucia G., Frenk



- C. S., Gao L., Jenkins A., Kauffmann G., Navarro J. F., Yoshida N., 2006, *MNRAS*, 365, 11
- De Lucia G., Springel V., White S. D. M., Croton D., Kauffmann G., 2006, *MNRAS*, 366, 499
- Di Matteo P., Bournaud F., Martig M., Combes F., Melchior A.-L., Semelin B., 2008, *A&A*, 492, 31
- Dutton A. A., Mendel J. T., Simard L., 2012, *MNRAS*, 422, L33
- Efstathiou G., Lake G., Negroponte J., 1982, *MNRAS*, 199, 1069
- Elmegreen B. G., 2004, *MNRAS*, 354, 367
- Faber S. M., 1973, *ApJ*, 179, 731
- Ferreras I., La Barbera F., de la Rosa I. G., Vazdekis A., de Carvalho R. R., Falcón-Barroso J., Ricciardelli E., 2013, *MNRAS*, 429, L15
- Feulner G., Gabasch A., Salvato M., Drory N., Hopp U., Bender R., 2005, *ApJL*, 633, L9
- Fontanot F., 2014, *MNRAS*, 442, 3138
- Fontanot F., De Lucia G., Monaco P., Somerville R. S., Santini P., 2009, *MNRAS*, 397, 1776
- Foster A. R., Ji L., Smith R. K., Brickhouse N. S., 2012, *ApJ*, 756, 128
- Gallazzi A., Charlot S., Brinchmann J., White S. D. M., Tremonti C. A., 2005, *MNRAS*, 362, 41
- Geisler D., Wallerstein G., Smith V. V., Casetti-Dinescu D. I., 2007, *pasp*, 119, 939
- Granato G. L., Lacey C. G., Silva L., Bressan A., Baugh C. M., Cole S., Frenk C. S., 2000, *ApJ*, 542, 710
- Greggio L., 2005, *A&A*, 441, 1055
- Greggio L., Renzini A., 1983, *A&A*, 118, 217
- Grevesse N., Noels A., Sauval A. J., 1996, in Holt S. S., Sonneborn G., eds, *Cosmic Abundances Vol. 99 of Astronomical Society of the Pacific Conference Series, Standard Abundances*. p. 117
- Häring N., Rix H.-W., 2004, *ApJL*, 604, L89
- Hirschi R., Meynet G., Maeder A., 2005, *A&A*, 433, 1013
- Iwamoto K., Brachwitz F., Namoto K., Kishimoto N., Umeda H., Hix W. R., Thielemann F., 1999, *ApJS*, 125, 439
- Jarosik N., Bennett C. L., Dunkley J., Gold B., Greason M. R., Halpern M., Hill R. S., Hinshaw G., et al. 2011, *ApJS*, 192, 14
- Jiménez N., Cora S. A., Bassino L. P., Tecce T. E., Smith Castelli A. V., 2011, *MNRAS*, 417, 785
- Karakas A. I., 2010, *MNRAS*, 403, 1413
- Kimm T., Yi S. K., Khochfar S., 2011, *ApJ*, 729, 11
- Kirk H., Myers P. C., 2011, *ApJ*, 727, 64
- Kobayashi C., Umeda H., Nomoto K., Tominaga N., Ohkubo T., 2006, *ApJ*, 653, 1145
- Köppen J., Weidner C., Kroupa P., 2007, *MNRAS*, 375, 673
- Kormendy J., Kennicutt Jr. R. C., 2004, *araa*, 42, 603
- Kroupa P., 2001, *MNRAS*, 322, 231
- Kroupa P., Boily C. M., 2002, *MNRAS*, 336, 1188
- Kroupa P., Weidner C., 2003, *ApJ*, 598, 1076
- Kroupa P., Weidner C., Pflamm-Altenburg J., Thies I., Dabringhausen J., Marks M., Maschberger T., 2013, *The Stellar and Sub-Stellar Initial Mass Function of Simple and Composite Populations*. Oswalt, T. D. and Gilmore, G., p. 115
- Kuntschner H., 2000, *MNRAS*, 315, 184
- La Barbera F., Ferreras I., Vazdekis A., de la Rosa I. G., de Carvalho R. R., Trevisan M., Falcón-Barroso J., Ricciardelli E., 2013, *MNRAS*, 433, 3017
- Lacey C. G., Baugh C. M., Frenk C. S., Silva L., Granato G. L., Bressan A., 2008, *MNRAS*, 385, 1155
- Lada C. J., Lada E. A., 2003, *MNRAS*, 41, 57
- Lagos C. D. P., Cora S. A., Padilla N. D., 2008, *MNRAS*, 388, 587
- Lagos C. D. P., Padilla N. D., Cora S. A., 2009, *MNRAS*, 397, L31
- Larsen S., 2002, *AJ*, 124, 1393
- Li W., Leaman J., Chornock R., Filippenko A. V., Poznanski D., Ganeshalingam M., Wang X., Modjaz M., Jha S., Foley R. J., Smith N., 2011, *MNRAS*, 412, 1441
- Lia C., Portinari L., Carraro G., 2002, *MNRAS*, 330, 821
- Lucatello S., Gratton R. G., Beers T. C., Carretta E., 2005, *ApJ*, 625, 833
- Malbon R. K., Baugh C. M., Frenk C. S., Lacey C. G., 2007, *MNRAS*, 382, 1394
- Marigo P., Girardi L., 2007, *A&A*, 469, 239
- Marigo P., Girardi L., Bressan A., Groenewegen M. A. T., Silva L., Granato G. L., 2008, *A&A*, 482, 883
- Marks M., Kroupa P., Dabringhausen J., Pawlowski M. S., 2012, *MNRAS*, 422, 2246
- Matteucci F., 1994, *A&A*, 288, 57
- Matteucci F., Greggio L., 1986, *A&A*, 154, 279
- Mattila S., Dahlen T., Efstathiou A., Kankare E., Melinder J., Alonso-Herrero A., Pérez-Torres M. Á., Ryder S., Väisänen P., Östlin G., 2012, *ApJ*, 756, 111
- Melinder J., Dahlen T., Mencia Trinchant L., stlin G., Mattila S., Sollerman J., Fransson C., Hayes M., Kankare E., Nasoudi-Shoar S., 2012, *A&A*, 545, 96
- Menci N., Cavaliere A., Fontana A., Giallongo E., Poli F., Vitorini V., 2004, *ApJ*, 604, 12
- Nagashima M., Lacey C. G., Baugh C. M., Frenk C. S., Cole S., 2005, *MNRAS*, 358, 1247
- Nagashima M., Lacey C. G., Okamoto T., Baugh C. M., Frenk C. S., Cole S., 2005, *MNRAS*, 363, L31
- Neistein E., van den Bosch F. C., Dekel A., 2006, *MNRAS*, 372, 933
- Nomoto K., Tominaga N., Umeda H., Kobayashi C., Maeda K., 2006, *Nuclear Physics A*, 777, 424
- Padilla N. D., Salazar-Albornoz S., Contreras S., Cora S. A., Ruiz A. N., 2014, *MNRAS*, 443, 2801
- Padovani P., Matteucci F., 1993, *ApJ*, 416, 26
- Panther B., Jimenez R., Heavens A. F., Charlot S., 2007, *MNRAS*, 378, 1550
- Pérez-González P. G., Trujillo I., Barro G., Gallego J., Zamorano J., Conselice C. J., 2008, *ApJ*, 687, 50
- Pipino A., Devriendt J. E. G., Thomas D., Silk J., Kaviraj S., 2009, *A&A*, 505, 1075
- Pipino A., Matteucci F., 2004, *MNRAS*, 347, 968
- Recchi S., Calura F., Kroupa P., 2009, *A&A*, 499, 711
- Renzini A., Buzzoni A., 1986, in Chiosi C., Renzini A., eds, *Spectral Evolution of Galaxies Vol. 122 of Astrophysics and Space Science Library, Global properties of stellar populations and the spectral evolution of galaxies*. pp 195–231
- Romano D., Karakas A. I., Tosi M., Matteucci F., 2010, *A&A*, 522, A32
- Ruiz A. N., Cora S. A., Padilla N. D., Domínguez M. J., Tecce T. E., Orsi Á., Yaryura Y. C., García Lambas D., Gargiulo I. D., Muñoz Arancibia A. M., 2014, *arxiv:1310.7034*
- Saglia R. P., Maraston C., Thomas D., Bender R., Colless M., 2002, *ApJL*, 579, L13
- Salpeter E. E., 1955, *ApJ*, 121, 161
- Sánchez-Blázquez P., Gorgas J., Cardiel N., González J. J., 2006, *A&A*, 457, 787
- Sani E., Lutz D., Risaliti G., Netzer H., Gallo L. C., Trakhtenbrot B., Sturm E., Boller T., 2010, *MNRAS*, 403, 1246



Shadmehri M., 2004, MNRAS, 354, 375  
 Sobral D., Best P. N., Smail I., Mobasher B., Stott J., Nisbet D., 2014, MNRAS, 437, 3516  
 Somerville R. S., Hopkins P. F., Cox T. J., Robertson B. E., Hernquist L., 2008, MNRAS, 391, 481  
 Spolaor M., Kobayashi C., Forbes D. A., Couch W. J., Hau G. K. T., 2010, MNRAS, 408, 272  
 Springel V., 2005, MNRAS, 364, 1105  
 Springel V., White S. D. M., Tormen G., Kauffmann G., 2001, MNRAS, 328, 726  
 Tecce T. E., Cora S. A., Tissera P. B., Abadi M. G., Lagos C. D. P., 2010, MNRAS, 408, 2008  
 Thies I., Kroupa P., 2007, ApJ, 671, 767  
 Thies I., Kroupa P., 2008, MNRAS, 390, 1200  
 Thomas D., 1999, MNRAS, 306, 655  
 Thomas D., Maraston C., 2003, A&A, 401, 429  
 Thomas D., Maraston C., Bender R., Mendes de Oliveira C., 2005, ApJ, 621, 673  
 Thomas D., Maraston C., Schawinski K., Sarzi M., Silk J., 2010, MNRAS, 404, 1775  
 Tinsley B. M., 1976, ApJ, 208, 797  
 Tinsley B. M., 1979, ApJ, 229, 1046  
 Tortora C., Romanowsky A. J., Napolitano N. R., 2013, ApJ, 765, 8  
 Trager S. C., Faber S. M., Dressler A., 2008, MNRAS, 386, 715  
 Trager S. C., Faber S. M., Worthey G., González J. J., 2000, AJ, 119, 1645  
 Treu T., Auger M. W., Koopmans L. V. E., Gavazzi R., Marshall P. J., Bolton A. S., 2010, ApJ, 709, 1195  
 van Dokkum P. G., Conroy C., 2010, NAT, 468, 940  
 van Dokkum P. G., Conroy C., 2012, ApJ, 760, 70  
 Weidner C., Ferreras I., Vazdekis A., La Barbera F., 2013, MNRAS, 435, 2274  
 Weidner C., Kroupa P., Larsen S. S., 2004, MNRAS, 350, 1503  
 Weidner C., Kroupa P., Pflamm-Altenburg J., 2011, MNRAS, 412, 979  
 Weidner C., Kroupa P., Pflamm-Altenburg J., 2013, MNRAS, 434, 84  
 Weidner C., Kroupa P., Pflamm-Altenburg J., Vazdekis A., 2013, MNRAS, 436, 3309  
 White S. D. M., Rees M. J., 1978, MNRAS, 183, 341  
 Woosley S. E., Weaver T. A., 1995, ApJS, 101, 181  
 Worthey G., Faber S. M., Gonzalez J. J., 1992, ApJ, 398, 69  
 Worthey G., Tang B., Serven J., 2013, arxiv:1303.2603  
 Yates R. M., Henriques B., Thomas P. A., Kauffmann G., Johansson J., White S. D. M., 2013, arxiv:1305.7231

This paper has been typeset from a  $\text{\LaTeX}$  file prepared by the author.

## APPENDIX A: FREE PARAMETERS AND ANALYTIC RECIPES IN THE MODEL

In the present appendix, we give a short description of the role of each of the free parameters involved in the model SAG and the recipes used to follow the formation and evolution of galaxies.

The efficiency of star formation,  $\alpha_{\text{SF}}$ , is a free parameter involved in the quiescent mode of star formation and follows the ex-

pression proposed by Croton et al. (2006), that is,

$$\frac{dM_{\star}}{dt} = \alpha \frac{M_{\text{cold}} - M_{\text{cold,crit}}}{t_{\text{dyn}}}, \quad (\text{A1})$$

with

$$M_{\text{cold,crit}} = 3.8 \times 10^9 \left( \frac{V_{\text{vir}}}{200 \text{ km s}^{-1}} \right) \left( \frac{3R_{\text{disc}}}{10 \text{ kpc}} \right) M_{\odot}, \quad (\text{A2})$$

where  $t_{\text{dyn}} = V_{\text{vir}}/3R_{\text{disc}}$  is the dynamical time of the galaxy,  $V_{\text{vir}}$  the circular velocity at the virial radius and  $R_{\text{disc}}$  the disc scale length (Tecce et al. 2010). If the mass of cold gas exceed  $M_{\text{cold,crit}}$ , star formation occurs.

The SNe feedback efficiency,  $\varepsilon$ , is a free parameter that controls the amount of cold gas reheated by the energy generated by SNe CC. The amount of reheated mass produced by a star forming event that generates a stellar population of mass  $\Delta M_{\star}$  is assumed to be

$$\Delta M_{\text{reheated}} = \frac{4}{3} \varepsilon \frac{\eta E}{V_{\text{vir}}^2} \Delta M_{\star} \quad (\text{A3})$$

where  $E = 10^{51} \text{ erg s}^{-1}$  is the energy released by a SNe, and  $\eta$  is the number of SNe which depends on the IMF adopted, estimated as

$$\eta = \frac{\int_0^8 \phi(m) m dm}{\int_0^{\infty} \phi(m) dm}, \quad (\text{A4})$$

where  $\phi(m)$  is the adopted IMF and  $m$  the stellar mass. This quantity is constant for the Salpeter IMF (models SAGS-c1 and SAGS-c2), and varies accordingly to the adopted slope of TH-IGIMF in each event of star formation for models SAGTH5B2, SAGTH5B21 and SAGTH100B2. The SNe feedback from stars in the disc and in the bulge is treated separately. The efficiency  $\varepsilon$  of eq. A3 corresponds to stars borned in the disc, and a new free parameter is introduced to regulate the SN feedback from stars in the bulge, to which we refer to as  $\varepsilon_{\text{bulge}}$ . In both cases, the amount of reheated mass is given by eq. A3.

There are two free parameters related to the growth of the BHs in the model. In first place, a BH is fed by the inflow of cold gas provided by perturbations to the gaseous disc resulting from galaxy mergers or disc instabilities. When a galaxy merger occurs, the central BHs are assumed to merge instantly. In all the versions of SAG calibrated for this work, a fraction of the cold gas from the merger remnant,  $f_{\text{BH}}$ , is supplied for the BH growth as

$$\Delta M_{\text{BH}} = f_{\text{BH}} \frac{M_{\text{sat}}}{M_{\text{cen}}} \frac{M_{\text{cold,sat}} + M_{\text{cold,cen}}}{(1 + 280 \text{ km s}^{-1}/V_{\text{vir}})^2} \quad (\text{A5})$$

where  $M_{\text{cen}}$  and  $M_{\text{sat}}$  are the masses of the merging central and satellite galaxies, and  $M_{\text{cold,cen}}$  and  $M_{\text{cold,sat}}$  are their corresponding masses of cold gas. When a starburst is triggered through a disk instability occurring in a galaxy, only the cold gas of the unstable galaxy is involved. The BH accretes cold gas gradually as long as there is bulge cold gas available (see Subsection 4.2). In the latter cases, the BH growth and star formation in starburst mode are coupled in such a way that their actions, together with SNe feedback from the stars formed in the bulge, determine the duration of the starburst. In second place, BHs grow from hot gas during the gas cooling processes taking place in central galaxies (type 0) as

$$\frac{dM_{\text{BH}}}{dt} = \kappa_{\text{AGN}} \frac{M_{\text{BH}}}{10^8 M_{\odot}} \frac{f_{\text{hot}}}{0.1} \left( \frac{V_{\text{vir}}}{200 \text{ km s}^{-1}} \right)^2 \quad (\text{A6})$$

where  $f_{\text{hot}} = M_{\text{hot}}/M_{\text{vir}}$ , being  $M_{\text{hot}}$  and  $M_{\text{vir}}$  the hot gas and virial

masses, respectively; the free parameter  $\kappa_{\text{AGN}}$  is the efficiency of accretion.

The last two free parameters of the calibration process are the fraction of binaries,  $A_{\text{bin}}$ , that originates SNe Ia, already introduced in Subsection 2.2.3, and the factor involved in the distance scale of perturbation to trigger disc instabilities,  $f_{\text{pert}}$  (see Subsection 2.2.2).